

CDNNs: The coupled deep neural networks for coupling of the Stokes and Darcy-Forchheimer problems ^{*}

Jing Yue^a, Jian Li ^{†a}, and Wen Zhang^a

^a*School of Electrical and Control Engineering, School of Mathematics and Data Science, Shaanxi University of Science and Technology, Xi'an*

Abstract

In this article, we present an efficient deep learning method called coupled deep neural networks (CDNNs) for coupled physical problems. Our method compiles the interface conditions of the coupled PDEs into the networks properly and can be served as an efficient alternative to the complex coupled problems. To impose energy conservation constraints, the CDNNs utilize simple fully connected layers and a custom loss function to perform the model training process as well as the physical property of the exact solution. The approach can be beneficial for the following reasons: Firstly, we sampled randomly and only input spatial coordinates without being restricted by the nature of samples. Secondly, our method is meshfree which makes it more efficient than the traditional methods. Finally, our method is parallel and can solve multiple variables independently at the same time. We give the theory to guarantee the convergence of the loss function and the convergence of the neural networks to the exact solution. Some numerical experiments are performed and discussed to demonstrate the performance of the proposed method.

Key words: Scientific computing, Machine learning, the Stokes equations, Darcy-Forchheimer problems, Beaver-Joseph-Saffman interface condition.

1 Introduction

The fluid flow between porous media and free-flow zones has extensive applications in hydrology, environmental science, and biofluid dynamics. A lot of researchers derive suitable mathematical and numerical models for fluid movement. The system can be viewed as a coupled problem with two physical systems interacting across an interface. The simplest mathematical formulation for the coupled problem is coupling of the Stokes and Darcy flow with proper interface conditions. The most suitable and popular interface conditions are called Beavers-Joseph-Saffman conditions

^{*}.

[†]Corresponding author(Jian Li) email: jianli@sust.edu.cn; jiaaanli@gmail.com.

[1]. However, Darcy’s law only provides a linear relationship between the gradient of pressure and velocity in the coupled model, which usually fails for complex physical problems. Forchheimer [2] conducted flow experiments in sand packs and recognized that for moderate Reynolds numbers ($Re > 0.1$ approximately), Darcy’s law is not adequate. He found that the pressure gradient and Darcy velocity should satisfy the Darcy-Forchheimer law. Since the great attention has received in the coupled model, a large number of traditional methods have been devoted to the coupled Stokes and Darcy flows problems [3, 4, 5, 6, 7, 8, 9, 10, 11, 12, 13]. However, the difficulty of the complicated high dimensional coupled problems causes the limitation of traditional methods.

Owing to the enormous potential in approximating high-dimensional nonlinear maps [17, 18, 19, 20, 21, 22, 23, 24], deep learning has attracted growing attention in many applications, such as image, speech, text recognition and scientific computing [14, 15, 16]. Many works have arisen based on the function approximation capabilities of the feed-forward fully-connected neural network to solve initial/boundary value problems [31, 32, 33, 34] in the past decades. The solution to the system of equations can be obtained by minimizing the loss function, which typically consists of the residual error of the governing Partial Differential Equations (PDEs) along with initial/boundary values. Recently, Raissi *etc.*[35, 36, 37] developed Physics Informed Neural Networks (PINNs) [38, 39, 40, 41, 42, 43]. Moreover, Sirignano and Spiliopoulos proposed the Deep learning Galerkin Method [45] for solving high dimensional PDEs. Additionally, some recent works have successfully solved the second-order linear elliptic equations and the high dimensional Stokes problems [25, 26, 27, 28]. Although several excellent works have been performed in applying deep learning to solve PDEs, the topic for solving complicated coupled interface problems remains to be investigated.

Considering the performance of deep learning for solving PDEs, our contribution is to design the CDNNs as an efficient alternative model for complicated coupled physical problems. We can encode any underlying physical laws naturally as prior information to obey the law of physics. To satisfy the differential operators, boundary conditions and divergence conditions, we train the neural networks on batches of randomly sampled points. The method only inputs random sampling spatial coordinates without considering the nature of samples. Notably, we take the interface conditions as the constraint for the CDNNs. The approach is parallel and solves multiple variables independently at the same time. Specially, the optimal solution can be obtained by using the appropriate optimization method instead of a linear combination of basic functions. Further more, we validate the convergence of the loss function under certain conditions and the convergence of the CDNNs to the exact solution. Several numerical experiments are conducted to investigate the performance of the CDNNs.

The article is organized as follows: Section 2 introduces the coupled model and the relation methodology. Section 3 discusses the convergence of the loss function $J(\bar{\mathbf{U}})$ and the convergence of the CDNNs to the exact solution. Section 4 reveals some numerical experiments to illustrate the efficiency of the CDNNs. The article ends with conclusion in section 5.

2 Methodology

Let Ω_S and Ω_D be two bounded and simply connected polygonal domains in \mathbb{R}^2 such that $\partial\Omega_S \cap \partial\Omega_D = \Gamma \neq \emptyset$ and $\Omega_S \cap \Omega_D = \emptyset$. Then, let $\Gamma_S := \partial\Omega_S \setminus \Gamma$, $\Gamma_D := \partial\Omega_D \setminus \Gamma$ and \mathbf{n}_S as the unit normal vector pointing from Ω_S to Ω_D , \mathbf{n}_D as the unit normal vector pointing from Ω_D to Ω_S , on the interface Γ we have $\mathbf{n}_D = -\mathbf{n}_S$. In addition, \mathbf{t} represents the unit tangential vector along the interface Γ . Figure 1 gives a schematic representation of the geometry.

When kinematic effects surpass viscous effects in a porous medium, the Darcy velocity \mathbf{u}_D and the pressure gradient ∇p_D does not satisfy a linear relation. Instead, a nonlinear approximation, known as the Darcy-Forchheimermodel, is considered. When it is imposed on the porous medium Ω_D with homogeneous Dirichlet boundary condition on Γ_D the equations read:

$$\nabla \cdot \mathbf{u}_D = f_D, \quad \text{in } \Omega_D, \quad (1)$$

$$\frac{\mu}{\rho} \mathbf{K}^{-1} \mathbf{u}_D + \frac{\beta}{\rho} |\mathbf{u}_D| \mathbf{u}_D + \nabla p_D = \mathbf{g}_D, \quad \text{in } \Omega_D, \quad (2)$$

$$p_D = 0, \quad \text{on } \partial\Omega_D \setminus \Gamma, \quad (3)$$

where \mathbf{K} is the permeability tensor, assumed to be uniformly positive definite and bounded, ρ is the density of the fluid, μ is its viscosity and β is a dynamic viscosity, all assumed to be positive constants. In addition, \mathbf{g}_D and f_D are source terms. We remark that in this context we exploit homogeneous Dirichlet boundary condition, in fact, we can also consider homogeneous Neumann boundary condition, i.e., $\mathbf{u}_D \cdot \mathbf{n}_D = 0$ on Γ_D and the arguments used in this paper are still true.

The fluid motion in Ω_S is described by the Stokes equations:

$$-\nu \Delta \mathbf{u}_S + \nabla p_S = \mathbf{f}_S, \quad \text{in } \Omega_S, \quad (4)$$

$$\nabla \cdot \mathbf{u}_S = 0, \quad \text{on } \Omega_S, \quad (5)$$

$$\mathbf{u}_S = 0, \quad \text{on } \partial\Omega_S \setminus \Gamma, \quad (6)$$

where $\nu > 0$ denotes the viscosity of the fluid.

On the interface, we prescribe the following interface conditions

$$\mathbf{u}_S \cdot \mathbf{n}_S = \mathbf{u}_D \cdot \mathbf{n}_S, \quad \text{on } \Gamma, \quad (7)$$

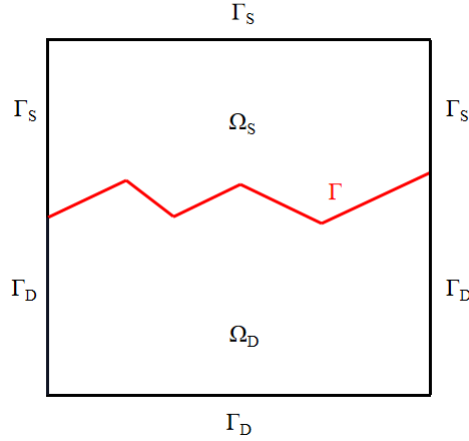
$$p_S - \nu \mathbf{n}_S \frac{\partial \mathbf{u}_S}{\partial \mathbf{n}_S} = p_D, \quad \text{on } \Gamma, \quad (8)$$

$$-\nu \mathbf{t} \frac{\partial \mathbf{u}_S}{\partial \mathbf{n}_S} = G \mathbf{u}_S \cdot \mathbf{t}, \quad \text{on } \Gamma. \quad (9)$$

Condition (7) represents continuity of the fluid velocity's normal components, (8) represents the balance of forces acting across the interface, and (9) is the Beaver-Joseph-Saffman condition [46]. The constant $G > 0$ is given and is usually obtained from experimental data.

For notational brevity, we set $\bar{\mathbf{u}} = (\mathbf{u}_S, \mathbf{u}_D, p_S, p_D)$ and recall the classical Sobolev spaces

$$\mathbb{X}_S^0 = \{v_S \in [H^1(\Omega_S)]^d : v_S|_{\Gamma_S} = \mathbf{0}\},$$

Figure 1: Coupled domain with interface Γ .

$$\mathbb{Y}_D = \{q_D \in [W^{1,3/2}(\Omega_D)]^2 : q_D|_{\Gamma_D} = 0\},$$

$$\mathbb{X}_S = \{v_S \in \mathbb{X}_S^0 : \text{div } v_S = 0\},$$

where

$$H^k(\Omega) = \left\{ v \in L^2(\Omega) : D_w^\alpha v \in L^2(\Omega), \forall \alpha : |\alpha| \leq k \right\},$$

and their norm

$$\|v\|_k = \sqrt{(v, v)_k} = \left\{ \sum_{|\alpha|=0}^k \int_{\Omega} (D_w^\alpha v)^2 dx \right\}^{\frac{1}{2}}, \quad \|v\|_{W_{k,p}} = \left\{ \sum_{|\alpha| \leq k} \|v\|_{L^p}^p \right\}^{1/p}.$$

Particularly,

$$\|v\|_k = \|v\|_{W^{k,2}}$$

where $k > 0$ is a positive integer and $\|v\|_0$ denotes the norm on $L^2(\Omega)$ or $(L^2(\Omega))^2$, $D_w^\alpha v$ is the generalized derivative of v . Moreover, $(\cdot, \cdot)_D$ represents the inner product in the domain D and $\langle \cdot, \cdot \rangle$ represents the inner product on the interface Γ .

To solve coupling of the Stokes and Darcy-Forchheimer problems, we propose the CDNNs in Figure 2. Further more, we give observations of the state variable $\bar{\mathbf{U}}(x; \theta) = (\mathbf{U}_S(x; \theta_1), \mathbf{U}_D(x; \theta_2), P_S(x; \theta_3), P_D(x; \theta_4))$, which is the neural network solution to the coupled Stokes and Darcy-Forchheimer problem (1)-(9), (θ_1, θ_3) and (θ_2, θ_4) are the stacked parameters of θ for Stokes and Darcy respectively. The following constrained optimization procedure aims to reconstruct the parameters θ by minimizing the loss function

$$J[\bar{\mathbf{U}}] = J_{\Omega_S \setminus \Gamma}[\bar{\mathbf{U}}] + J_{\Omega_D \setminus \Gamma}[\bar{\mathbf{U}}] + J_{\Gamma}[\bar{\mathbf{U}}]. \quad (10)$$

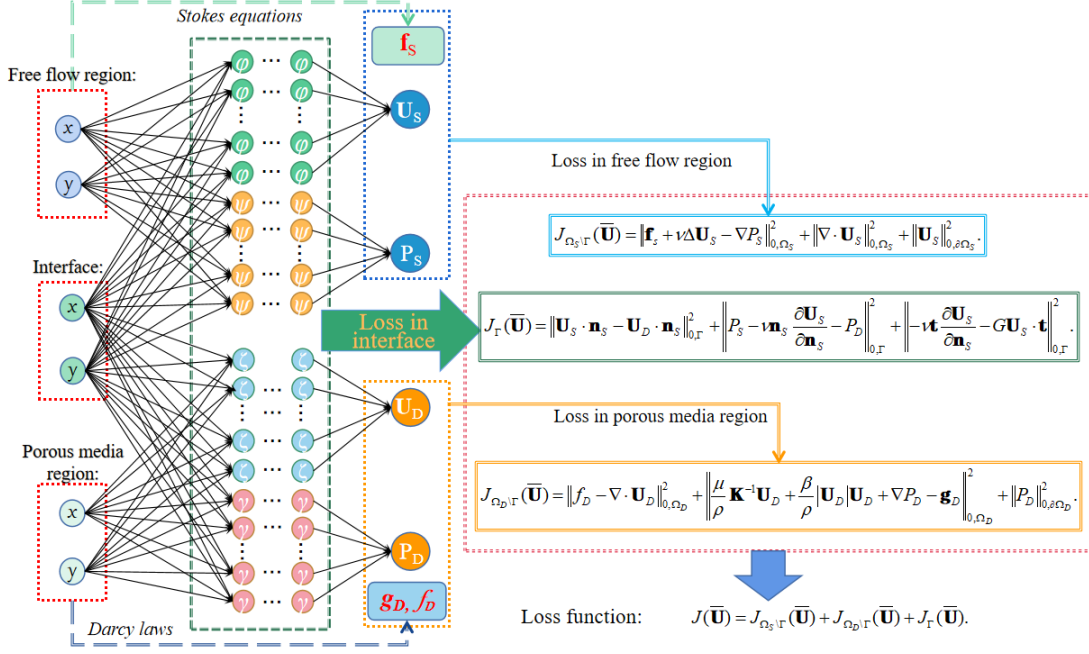


Figure 2: The structure of the CDNNs.

where

$$\begin{aligned}
J_{\Omega_S \setminus \Gamma}(\bar{\mathbf{U}}) &= \left\| f_S + \nu \Delta \mathbf{U}_S(x; \theta_1) - \nabla P_S(x; \theta_3) \right\|_{0, \Omega_S, \omega_1}^2 \\
&\quad + \left\| \nabla \cdot \mathbf{U}_S(x; \theta_1) \right\|_{0, \Omega_S, \omega_1}^2 + \left\| \mathbf{U}_S(x; \theta_1) \right\|_{0, \partial \Omega_S \setminus \Gamma, \omega_2}^2 \\
J_{\Omega_D \setminus \Gamma}(\bar{\mathbf{U}}) &= \left\| f_D - \nabla \cdot \mathbf{U}_D(x; \theta_2) \right\|_{0, \Omega_D, \omega_1}^2 \\
&\quad + \left\| \frac{\mu}{\rho} \mathbf{K}^{-1} \mathbf{U}_D(x; \theta_2) + \frac{\beta}{\rho} |\mathbf{U}_D(x; \theta_2)| \mathbf{U}_D(x; \theta_2) + \nabla P_D(x; \theta_4) - \mathbf{g}_D \right\|_{0, \Omega_D, \omega_1}^2 \\
&\quad + \left\| P_D(x; \theta_4) \right\|_{0, \partial \Omega_D \setminus \Gamma, \omega_2}^2 \\
J_{\Gamma}(\bar{\mathbf{U}}) &= \left\| \mathbf{U}_S(x; \theta_1) \cdot \mathbf{n}_S - \mathbf{U}_D(x; \theta_2) \cdot \mathbf{n}_S \right\|_{0, \Gamma, \omega_3}^2 \\
&\quad + \left\| P_S(x; \theta_3) - \nu \mathbf{n}_S \frac{\partial \mathbf{U}_S(x; \theta_1)}{\partial \mathbf{n}_S} - P_D(x; \theta_4) \right\|_{0, \Gamma, \omega_3}^2 \\
&\quad + \left\| -\nu \mathbf{t} \frac{\partial \mathbf{U}_S(x; \theta_1)}{\partial \mathbf{n}_S} - G \mathbf{U}_S(x; \theta_1) \cdot \mathbf{t} \right\|_{0, \Gamma, \omega_3}^2
\end{aligned} \tag{11}$$

The nodal values of the parameters in the input layer admitted by the deep learning model. Furthermore, it should be noted that $J(\bar{\mathbf{U}})$ can measure how well the approximate solution satisfies differential operators, divergence conditions, boundary conditions and interface conditions. Notice

that

$$\|f(y)\|_{0,\mathcal{Y},\omega} = \int_{\mathcal{Y}} |f(y)|^2 \omega(y) dy,$$

where $\omega(y)$ is the probability density of y in \mathcal{Y} . Especially, if $J(\bar{\mathbf{U}}) = 0$ then $\bar{\mathbf{U}}$ is the solution to the coupled Stokes and Darcy-Forchheimer problems (1)-(9). Due to the infeasibility to estimate θ by directly minimizing $J(\bar{\mathbf{U}})$ when integrated over a higher dimensional region, so we apply a sequence of randomly sampled points from domain instead forming mesh grid. The main steps of the CDNNs for the coupled Stokes and Darcy-Forchheimer equations are presented as **Algorithm 1**. Another noticeable point is that the term $\nabla_{\theta} G(\theta^n, z^{(n)})$ is unbiased estimate of $\nabla_{\theta} J(\bar{\mathbf{U}}(\cdot; \theta^n))$ because the population parameters can be estimated by sample mathematical expectations.

3 Convergence

According to the definition of loss function $J(\bar{\mathbf{U}})$, it can measure how well $\bar{\mathbf{U}}$ satisfies the equations (1)-(9). Neural networks are a set of algorithms for classification and regression tasks inspired by the biological neural networks in brains. There have various types of neural networks with different neuron connection forms and architectures. According to the [20], if there is only one hidden layer and output, the set of functions implemented by following networks with m_1, m_2, m_3 and m_4 hidden units for coupling of the Stokes and Darcy-Forchheimer problems are

$$\begin{aligned} [\mathfrak{C}_{\mathbf{U}_S}^{m_1}(\varphi)]^d &= \left\{ \Theta(x) : \mathbb{R}^d \mapsto \mathbb{R}^d \mid \Theta(x) = \sum_{i=1}^{m_1} \beta_i \varphi \left(\sum_{j=1}^d \sigma_{j,i} x_j + c_i \right) \right\}, \\ [\mathfrak{C}_{\mathbf{U}_D}^{m_2}(\zeta)]^d &= \left\{ \Lambda(x) : \mathbb{R}^d \mapsto \mathbb{R}^d \mid \Lambda(x) = \sum_{i=1}^{m_2} \beta'_i \zeta \left(\sum_{j=1}^d \sigma'_{j,i} x_j + c'_i \right) \right\}, \\ \mathfrak{C}_{P_S}^{m_3}(\psi) &= \left\{ \Psi(t, x) : \mathbb{R}^d \mapsto \mathbb{R} \mid \Psi(x) = \sum_{i=1}^{m_3} \beta''_i \psi \left(\sum_{j=1}^d \sigma''_{j,i} x_j + c''_i \right) \right\}, \\ \mathfrak{C}_{P_D}^{m_4}(\gamma) &= \left\{ \Upsilon(t, x) : \mathbb{R}^d \mapsto \mathbb{R} \mid \Upsilon(x) = \sum_{i=1}^{m_4} \beta'''_i \gamma \left(\sum_{j=1}^d \sigma'''_{j,i} x_j + c'''_i \right) \right\}, \end{aligned}$$

where $\Theta(x) = (\Theta_1(x), \Theta_2(x), \dots, \Theta_d(x))$, $\Lambda(x) = (\Lambda_1(x), \Lambda_2(x), \dots, \Lambda_d(x))$, φ, ζ, ψ and γ are the shared activation functions of the hidden units in $\mathcal{C}^2(\Omega)$, bounded and non-constant. x_j is input, $\beta_i, \beta'_i, \beta''_i, \beta'''_i, \sigma_{ji}, \sigma'_{ji}, \sigma''_{ji}$ and σ'''_{ji} are weights, c_i, c'_i, c''_i and c'''_i are thresholds of the neural networks.

More generally, we use the similar notation

$$[\mathfrak{C}_{\mathbf{U}_S}(\varphi)]^d \times [\mathfrak{C}_{\mathbf{U}_D}(\zeta)]^d \times \mathfrak{C}_{P_S}(\psi) \times \mathfrak{C}_{P_D}(\gamma)$$

for the multi layer neural networks with arbitrarily large number of hidden units m_1, m_2, m_3 and m_4 . In particular, the parameters and the activation function in each dimension of $[\mathfrak{C}_{\mathbf{U}_S}^{m_1}(\varphi)]^d$ or

Algorithm 1: The CDNNs for the coupled problems

Input: $\rho_{\omega_1}^{(n)} = \{x_S^n, x_D^n\}$, $\rho_{\omega_2}^{(n)} = \{r_S^n, r_D^n\}$, $\rho_{\omega_3}^{(n)} = \{r_\Gamma^n\}$, max iterations M , learning rate α
Output: θ_{n+1}

1. Randomly generated sample points $\rho^{(n)} = \{\rho_{\omega_1}^{(n)}, \rho_{\omega_2}^{(n)}, \rho_{\omega_3}^{(n)}\}$ from (Ω_S, Ω_D) , $(\partial\Omega_S \setminus \Gamma, \partial\Omega_D \setminus \Gamma)$ and Γ by the respective probability densities ω_1 , ω_2 and ω_3 ;
2. Initialize the parameters θ ;
3. **while** *iterations* $\leq M$ **do**
 read current;

$$G(\rho^{(n)}, \theta^n) = G_S(\rho^{(n)}, \theta^n) + G_D(\rho^{(n)}, \theta^n) + G_\Gamma(\rho^{(n)}, \theta^n),$$

where

$$\begin{aligned} G_S(\rho^{(n)}, \theta^n) &= \left(\mathbf{f}_S + \nu \Delta \mathbf{U}_S(x_S^n; \theta_1) - \nabla P_S(x_S^n; \theta_3) \right)^2 \\ &\quad + \left(\nabla \cdot \mathbf{U}_S(x_S^n; \theta_1) \right)^2 + \left(\mathbf{U}_S(r_S^n; \theta_1) \right)^2, \\ G_D(\rho^{(n)}, \theta^n) &= \left(\frac{\mu}{\rho} K^{-1} \mathbf{U}_D(x_D^n; \theta_2) + \frac{\beta}{\rho} |\mathbf{U}_D(x_D^n; \theta_2)| \mathbf{U}_D(x_D^n; \theta_2) + \nabla P_D(x_D^n; \theta_4) - \mathbf{g}_D \right)^2 \\ &\quad + \left(f_D - \nabla \cdot \mathbf{U}_D(x_D^n; \theta_2) \right)^2 + \left(P_D(r_D^n; \theta_4) \right)^2, \end{aligned}$$

and

$$\begin{aligned} G_\Gamma(\rho^{(n)}, \theta^n) &= \left(\mathbf{U}_S(x; \theta_1) \cdot \mathbf{n}_S - \mathbf{U}_D(x; \theta_2) \cdot \mathbf{n}_S \right)^2 \\ &\quad + \left(P_S(x; \theta_3) - \nu \mathbf{n}_S \frac{\partial \mathbf{U}_S(x; \theta_1)}{\partial \mathbf{n}_S} - P_D(x; \theta_4) \right)^2 \\ &\quad + \left(-\nu \mathbf{t} \frac{\partial \mathbf{U}_S(x; \theta_1)}{\partial \mathbf{n}_S} - G \mathbf{U}_S(x; \theta_1) \cdot \mathbf{t} \right)^2, \end{aligned}$$

and

$$\theta^{n+1} = \theta_n - \alpha \nabla_\theta G(\rho^{(n)}, \theta^n).$$

if $\lim_{n \rightarrow \infty} \|\nabla_\theta G(\rho^{(n)}, \theta_n)\| = 0$ **then**

 | return the parameters θ_{n+1} ;

else

 | go back to the beginning of current section.

$[\mathfrak{C}_{\mathbf{U}_D}^{\mathfrak{m}_2}(\zeta)]^d$ are same as before, we set n as the number of the neurons in numerical experiments. Then the parameters of the CDNNs can be formalized as follows

$$\begin{aligned}\theta_1^k &= (\beta_1, \dots, \beta_n, \sigma_{11}, \dots, \sigma_{dn}, c_1, \dots, c_n), \\ \theta_2^k &= (\beta'_1, \dots, \beta'_n, \sigma'_{11}, \dots, \sigma'_{dn}, c'_1, \dots, c'_n), \\ \theta_3 &= (\beta''_1, \dots, \beta''_n, \sigma''_{11}, \dots, \sigma''_{dn}, c''_1, \dots, c''_n), \\ \theta_4 &= (\beta'''_1, \dots, \beta'''_n, \sigma'''_{11}, \dots, \sigma'''_{dn}, c'''_1, \dots, c'''_n),\end{aligned}$$

where $k = 1, 2, \dots, d, \theta_1 \in \mathbb{R}^{(2+d)nd}, \theta_2 \in \mathbb{R}^{(2+d)nd}, \theta_3 \in \mathbb{R}^{(2+d)n}$ and $\theta_4 \in \mathbb{R}^{(2+d)n}$.

In the next two subsections, we prove that the neural network $\bar{\mathbf{U}}^n$ with n hidden units for $\mathbf{U}_S^n, \mathbf{U}_D^n, P_S^n$ and P_D^n satisfy the differential operators, boundary conditions, divergence conditions and interface conditions arbitrarily well for sufficiently large n . More importantly, we confirm that there exists $\bar{\mathbf{U}}^n \in [\mathfrak{C}_{\mathbf{U}_S}(\varphi)]^d \times [\mathfrak{C}_{\mathbf{U}_D}(\zeta)]^d \times \mathfrak{C}_{P_S}(\psi) \times \mathfrak{C}_{P_D}(\gamma)$ such that $J(\bar{\mathbf{U}}^n) \rightarrow 0$ as $n \rightarrow \infty$. Another significant consideration, we give the convergence of $\bar{\mathbf{U}}^n \rightarrow \bar{\mathbf{u}}$ as $n \rightarrow \infty$ where $\bar{\mathbf{u}}$ is the exact solution to the coupled equations (1)-(9).

3.1 Convergence of the loss function $J(\bar{\mathbf{U}})$

In this subsection, we prove the CDNNs $\bar{\mathbf{U}}$ can make the loss function $J(\bar{\mathbf{U}})$ arbitrarily small.

Assumption 3.1. $\nabla \mathbf{v}(x), \Delta \mathbf{v}(x)$ and $\nabla q(x)$ are locally Lipschitz with Lipschitz coefficient that they have at most polynomial growth on $\mathbf{v}(x)$ and $q(x)$. Then, for some constants $0 \leq q_i \leq \infty (i = 1, 2, 3, 4)$ we have

$$|\Delta \mathbf{V}(x; \theta) - \Delta \mathbf{v}(x)| \leq (|\nabla \mathbf{V}(x; \theta)|^{q_1/2} + |\nabla \mathbf{v}(x)|^{q_2/2}) |\nabla \mathbf{V}(x; \theta) - \nabla \mathbf{v}(x)|, \quad (12)$$

$$|\nabla Q(x; \theta) - \nabla q(x)| \leq (|Q(x; \theta)|^{q_3/2} + |q(x)|^{q_4/2}) |Q(x; \theta) - q(x)|, \quad (13)$$

$$|\nabla \mathbf{V}(x; \theta) - \nabla \mathbf{v}(x)| \leq (|\mathbf{V}(x; \theta)|^{q_5/2} + |\mathbf{v}(x)|^{q_6/2}) |\mathbf{V}(x; \theta) - \mathbf{v}(x)|. \quad (14)$$

Theorem 3.1. Under the Assumption 3.1, there exists a neural network $\bar{\mathbf{U}} \in [\mathfrak{C}_{\mathbf{U}_S}(\varphi)]^d \times [\mathfrak{C}_{\mathbf{U}_D}(\zeta)]^d \times \mathfrak{C}_{P_S}(\psi) \times \mathfrak{C}_{P_D}(\gamma)$, satisfying

$$J(\bar{\mathbf{U}}) \leq C\epsilon^2, \quad \forall \epsilon > 0, \quad (15)$$

where C depends on the data $\{\Omega_S, \Omega_D, \Gamma, \mu, \rho, \beta, K^{-1}, \omega_1, \omega_2, \omega_3, f_D, \mathbf{g}_D, \mathbf{f}_S\}$.

Proof. From Theorem 3 of [20], we obtain that there exists $\bar{\mathbf{U}} \in [\mathfrak{C}_{\mathbf{U}_S}(\varphi)]^d \times [\mathfrak{C}_{\mathbf{U}_D}(\zeta)]^d \times \mathfrak{C}_{P_S}(\psi) \times \mathfrak{C}_{P_D}(\gamma)$ which are uniformly 2-dense on compacts of $\mathcal{C}^2(\bar{\Omega}_S) \times \mathcal{C}^2(\bar{\Omega}_D) \times \mathcal{C}^1(\bar{\Omega}_S) \times \mathcal{C}^1(\bar{\Omega}_D)$. It means that for $\bar{\mathbf{u}}(x) \in \mathcal{C}^2(\bar{\Omega}_S) \times \mathcal{C}^2(\bar{\Omega}_D) \times \mathcal{C}^1(\bar{\Omega}_S) \times \mathcal{C}^1(\bar{\Omega}_D), \forall \epsilon > 0$, we confirm that

$$\max_{a \leq 2} \sup_{x \in \Omega_S} |\partial_x^a \mathbf{U}_S(x; \theta_1) - \partial_x^a \mathbf{u}_S(x)| < \epsilon, \quad (16)$$

$$\max_{a \leq 2} \sup_{x \in \Omega_D} |\partial_x^a \mathbf{U}_D(x; \theta_2) - \partial_x^a \mathbf{u}_D(x)| < \epsilon, \quad (17)$$

$$\sup_{x \in \Omega_S} |P_S(x; \theta_3) - p_S(x)| < \epsilon. \quad (18)$$

$$\sup_{x \in \Omega_D} |P_D(x; \theta_4) - p_D(x)| < \epsilon. \quad (19)$$

Firstly, we recall the form and discuss the convergence of $J_{\Omega_S \setminus \Gamma}(\bar{\mathbf{U}})$,

$$\begin{aligned} J_{\Omega_S \setminus \Gamma}(\bar{\mathbf{U}}) &= \left\| \mathbf{f}_S + \nu \Delta \mathbf{U}_S(x; \theta_1) - \nabla P_S(x; \theta_3) \right\|_{0, \Omega_S, \omega_1}^2 \\ &\quad + \left\| \nabla \cdot \mathbf{U}_S(x; \theta_1) \right\|_{0, \Omega_S, \omega_1}^2 + \left\| \mathbf{U}_S(x; \theta_1) \right\|_{0, \partial \Omega_S \setminus \Gamma, \omega_2}^2 \end{aligned} \quad (20)$$

According to the Assumption 3.1, by using the *Hölder* inequality and *Young* inequality, setting conjugate numbers r_1 and r_2 such that $\frac{1}{r_1} + \frac{1}{r_2} = 1$, it follows that

$$\begin{aligned} &\int_{\Omega_S} |\Delta \mathbf{U}(x; \theta_1) - \Delta \mathbf{u}(x)|^2 d\omega_1(x) \\ &\leq \int_{\Omega_S} \left(|\nabla \mathbf{U}(x; \theta_1)|^{l_1} + |\nabla \mathbf{u}(x)|^{l_2} \right) \left(\nabla \mathbf{U}(x; \theta_1) - \nabla \mathbf{u}(x) \right)^2 d\omega_1(x) \\ &\leq \left[\int_{\Omega_S} \left(|\nabla \mathbf{U}(x; \theta_1)|^{l_1} + |\nabla \mathbf{u}(x)|^{l_2} \right)^{r_1} d\omega_1(x) \right]^{1/r_1} \\ &\quad \times \left[\int_{\Omega_S} \left(\nabla \mathbf{U}(x; \theta_1) - \nabla \mathbf{u}(x) \right)^{2r_2} d\omega_1(x) \right]^{1/r_2} \\ &\leq \left[\int_{\Omega_S} \left(|\nabla \mathbf{U}(x; \theta_1) - \nabla \mathbf{u}(x)|^{l_1} + |\nabla \mathbf{u}(x)|^{l_1 \vee l_2} \right)^{r_1} d\omega_1(x) \right]^{1/r_1} \\ &\quad \times \left[\int_{\Omega_S} \left(\nabla \mathbf{U}(x; \theta_1) - \nabla \mathbf{u}(x) \right)^{2r_2} d\omega_1(x) \right]^{1/r_2} \\ &\leq C \left(\epsilon^{l_1} + \sup_{\Omega_S} |\nabla \mathbf{u}(x)|^{l_1 \vee l_2} \right) \epsilon^2, \end{aligned} \quad (21)$$

here we set $l_1 \vee l_2 = \max\{l_1, l_2\}$. In the same way,

$$\begin{aligned} &\int_{\Omega_S} \left| \nabla P_S(x; \theta_3) - \nabla p_S(x) \right|^2 d\omega_1(x) \\ &\leq \int_{\Omega_S} \left(|P_S(x; \theta_3)|^{l_3} + |p_S(x)|^{l_4} \right) \left(P_S(x; \theta_3) - p_S(x) \right)^2 d\omega_1(x) \\ &\leq \left[\int_{\Omega_S} \left(|P_S(x; \theta_3)|^{l_3} + |p_S(x)|^{l_4} \right)^{r_3} d\omega_1(x) \right]^{1/r_3} \times \left[\int_{\Omega_S} \left(P_S(x; \theta_3) - p_S(x) \right)^{2r_4} d\omega_1(x) \right]^{1/r_4} \\ &\leq \left[\int_{\Omega_S} \left(|P_S(x; \theta_3) - p_S(x)|^{l_3} + |p_S(x)|^{l_3 \vee l_4} \right)^{r_3} d\omega_1(x) \right]^{1/r_3} \times \left[\int_{\Omega_S} \left(P_S(x; \theta_3) - p_S(x) \right)^{2r_4} d\omega_1(x) \right]^{1/r_4} \\ &\leq C \left(\epsilon^{l_3} + \sup_{\Omega_S} |p_S(x)|^{l_3 \vee l_4} \right) \epsilon^2, \end{aligned} \quad (22)$$

where $\frac{1}{r_3} + \frac{1}{r_4} = 1$ and $l_3 \vee l_4 = \max\{l_3, l_4\}$.

For the boundary condition, we have

$$\int_{\partial\Omega_S \setminus \Gamma} |U_S(x; \theta_1) - u_S(x)|^2 d\omega_2(x) \leq C\epsilon^2. \quad (23)$$

Owing to (21) - (23), we can conclude that

$$\begin{aligned} J_{\Omega_S \setminus \Gamma}(\bar{\mathbf{U}}) &= \left\| \mathbf{f}_S + \nu \Delta \mathbf{U}_S(x; \theta_1) - \nabla P_S(x; \theta_3) \right\|_{0, \Omega_S, \omega_1}^2 \\ &\quad + \left\| \nabla \cdot \mathbf{U}_S(x; \theta_1) \right\|_{0, \Omega_S, \omega_1}^2 + \left\| \mathbf{U}_S(x; \theta_1) \right\|_{0, \partial\Omega_S \setminus \Gamma, \omega_2}^2 \\ &\leq \nu \left\| \Delta \mathbf{U}_S(x; \theta_1) - \Delta \mathbf{u}_S(x) \right\|_{0, \Omega_S, \omega_1}^2 + \left\| \nabla P_S(x; \theta_3) - \nabla p_S(x) \right\|_{0, \Omega_S, \omega_1}^2 \\ &\quad + \left\| \nabla \cdot \mathbf{U}_S(x; \theta_1) \right\|_{0, \Omega_S, \omega_1}^2 + \left\| \mathbf{U}_S(x; \theta_1) \right\|_{0, \partial\Omega_S \setminus \Gamma, \omega_2}^2 \\ &\leq \nu \int_{\Omega_S} |\Delta \mathbf{U}_S(x; \theta_1) - \Delta \mathbf{u}_S(x)|^2 d\omega_1(x) + \int_{\Omega_S} |\nabla P_S(x; \theta_3) - \nabla p_S(x)|^2 d\omega_1(x) \\ &\quad + \int_{\Omega_S} |\nabla \cdot \mathbf{u}_S(x)|^2 d\omega_1(x) + \int_{\Omega_S} \left| \nabla \cdot (\mathbf{U}_S(x; \theta_1) - \mathbf{u}_S(x)) \right|^2 d\omega_1(x) \\ &\quad + \int_{\partial\Omega_S \setminus \Gamma} |\mathbf{U}_S(x; \theta_1) - \mathbf{u}_S(x)|^2 d\omega_2(x) \\ &\leq C\epsilon^2. \end{aligned} \quad (24)$$

Next, we remain to prove the convergence of $J_{\Omega_D \setminus \Gamma}(\bar{\mathbf{U}})$ and $J_\Gamma(\bar{\mathbf{U}})$. We know that

$$\begin{aligned} J_{\Omega_D \setminus \Gamma}(\bar{\mathbf{U}}) &= \left\| f_D - \nabla \cdot \mathbf{U}_D(x; \theta_2) \right\|_{0, \Omega_D, \omega_1}^2 + \left\| P_D(x; \theta_4) \right\|_{0, \partial\Omega_D \setminus \Gamma, \omega_2}^2 \\ &\quad + \left\| \frac{\mu}{\rho} K^{-1} \mathbf{U}_D(x; \theta_2) + \frac{\beta}{\rho} |\mathbf{U}_D(x; \theta_2)| \mathbf{U}_D(x; \theta_2) + \nabla P_D(x; \theta_4) - \mathbf{g}_D \right\|_{0, \Omega_D, \omega_1}^2. \end{aligned} \quad (25)$$

From (19), we have

$$\begin{aligned} &\int_{\Omega_D} \left| \nabla P_D(x; \theta_4) - \nabla p_D(x) \right|^2 d\omega_1(x) \\ &\leq \int_{\Omega_D} \left(|P_D(x; \theta_4)|^{l_5} + |p_D(x)|^{l_6} \right) \left(P_D(x; \theta_4) - p_D(x) \right)^2 d\omega_1(x), \end{aligned} \quad (26)$$

which can be updated by using the Hölder inequality and Young inequality, thus we have

$$\begin{aligned} &\left[\int_{\Omega_D} \left(|P_D(x; \theta_4)|^{l_5} + |p_D(x)|^{l_6} \right)^{r_5} d\omega_1(x) \right]^{1/r_5} \\ &\quad \times \left[\int_{\Omega_D} (P_D(x; \theta_4) - p_D(x))^{2r_6} d\omega_1(x) \right]^{1/r_6} \\ &\leq \left[\int_{\Omega_D} \left(|P_D(x; \theta_4) - p_D(x)|^{l_5} + |p_D(x)|^{l_5 \vee l_6} \right)^{r_5} d\omega_1(x) \right]^{1/r_5} \\ &\quad \times \left[\int_{\Omega_D} (P_D(x; \theta_4) - p_D(x))^{2r_6} d\omega_1(x) \right]^{1/r_6} \\ &\leq C \left(\epsilon^{l_5} + \sup_{\Omega_D} |p_D(x)|^{l_5 \vee l_6} \right) \epsilon^2, \end{aligned} \quad (27)$$

where $\frac{1}{r_5} + \frac{1}{r_6} = 1$ and $l_5 \vee l_6 = \max\{l_5, l_6\}$.

Next we prove the boundedness of term $|\mathbf{U}_D(x; \theta_2)|\mathbf{U}_D(x; \theta_2)$,

$$\begin{aligned}
& \int_{\Omega_D} \left(|\mathbf{U}_D(x; \theta_2)|\mathbf{U}_D(x; \theta_2) - |\mathbf{u}_D(x)|\mathbf{u}_D(x) \right)^2 d\omega_1(x) \\
&= \int_{\Omega_D} \left(\mathbf{U}_D(x; \theta_2) \left(|\mathbf{U}_D(x; \theta_2)| - |\mathbf{u}_D(x)| \right) + |\mathbf{u}_D(x)| \left(\mathbf{U}_D(x; \theta_2) - \mathbf{u}_D(x) \right) \right)^2 d\omega_1(x) \\
&= \int_{\Omega_D} \left(\mathbf{U}_D(x; \theta_2) \left(|\mathbf{U}_D(x; \theta_2)| - |\mathbf{u}_D(x)| \right) \right)^2 d\omega_1(x) + \int_{\Omega_D} \left(|\mathbf{u}_D(x)| \left(\mathbf{U}_D(x; \theta_2) - \mathbf{u}_D(x) \right) \right)^2 d\omega_1(x) \\
&\quad + 2 \int_{\Omega_D} \left(|\mathbf{u}_D(x)|\mathbf{U}_D(x; \theta_2) \left(|\mathbf{U}_D(x; \theta_2)| - |\mathbf{u}_D(x)| \right) \left(\mathbf{U}_D(x; \theta_2) - \mathbf{u}_D(x) \right) \right) d\omega_1(x),
\end{aligned} \tag{28}$$

where

$$\begin{aligned}
& \int_{\Omega_D} \left(\mathbf{U}_D(x; \theta_2) \left(|\mathbf{U}_D(x; \theta_2)| - |\mathbf{u}_D(x)| \right) \right)^2 d\omega_1(x) \\
&\leq \left[\int_{\Omega_D} \left(\mathbf{U}_D(x; \theta_2) \right)^{2r_7} d\omega_1(x) \right]^{1/r_7} \times \left[\int_{\Omega_D} \left(|\mathbf{U}_D(x; \theta_2)| + |\mathbf{u}_D(x)| \right)^{2r_8} d\omega_1(x) \right]^{r_8} \\
&\leq \left[\int_{\Omega_D} \left(\left(\mathbf{U}_D(x; \theta_2) - \mathbf{u}_D(x) \right) + \mathbf{u}_D(x) \right)^{2r_7} d\omega_1(x) \right]^{1/r_7} \\
&\quad \times \left[\int_{\Omega_D} \left(|\mathbf{U}_D(x; \theta_2) - \mathbf{u}_D(x)| + |\mathbf{u}_D(x)| \right)^{2r_8} d\omega_1(x) \right]^{r_8},
\end{aligned} \tag{29}$$

by using the *Hölder* inequality and *Young* inequality, setting conjugate numbers r_7 and r_8 such that $\frac{1}{r_7} + \frac{1}{r_8} = 1$.

Similarly, we can obtain

$$\begin{aligned}
& \int_{\Omega_D} \left(|\mathbf{u}_D(x)| \left(\mathbf{U}_D(x; \theta_2) - \mathbf{u}_D(x) \right) \right)^2 d\omega_1(x) \\
&\leq \left[\int_{\Omega_D} \left(|\mathbf{u}_D(x)| \right)^{r_9} d\omega_1(x) \right]^{1/r_9} \times \left[\int_{\Omega_D} \left(\mathbf{U}_D(x; \theta_2) - \mathbf{u}_D(x) \right)^{2r_{10}} d\omega_1(x) \right]^{1/r_{10}},
\end{aligned} \tag{30}$$

here $\frac{1}{r_9} + \frac{1}{r_{10}} = 1$. Furthermore, we set $\frac{1}{r_{11}} + \frac{1}{r_{12}} = 1$ and $\frac{1}{r_{13}} + \frac{1}{r_{14}} = 1$,

$$\begin{aligned}
& \int_{\Omega_D} |\mathbf{u}_D(x)| \mathbf{U}_D(x; \theta_2) \left(|\mathbf{U}_D(x; \theta_2)| - |\mathbf{u}_D(x)| \right) \left(\mathbf{U}_D(x; \theta_2) - \mathbf{u}_D(x) \right) d\omega_1(x) \\
& \leq \left[\int_{\Omega_D} \left(\mathbf{U}_D(x; \theta_2) \left(|\mathbf{U}_D(x; \theta_2)| - |\mathbf{u}_D(x)| \right) \right)^{r_{11}} d\omega_1(x) \right]^{1/r_{11}} \\
& \quad \times \left[\int_{\Omega_D} \left(|\mathbf{u}_D(x)| \left(\mathbf{U}_D(x; \theta_2) - \mathbf{u}_D(x) \right) \right)^{r_{12}} d\omega_1(x) \right]^{1/r_{12}} \\
& \leq \left[\int_{\Omega_D} \left(\left(\mathbf{U}_D(x; \theta_2) - \mathbf{u}_D(x) \right) + \mathbf{u}_D(x) \right)^{r_{11}r_{13}} \right]^{1/r_{11}r_{13}} \\
& \quad \times \left[\int_{\Omega_D} \left(|\mathbf{U}_D(x; \theta_2) - \mathbf{u}_D(x)| + |\mathbf{u}_D(x)| \right)^{r_{11}r_{13}} d\omega_1(x) \right]^{1/r_{11}r_{13}} \\
& \quad \times \left[\int_{\Omega_D} |\mathbf{u}_D(x)|^{r_{12}r_{14}} d\omega_1(x) \right]^{1/r_{12}r_{14}} \times \left[\int_{\Omega_D} \left(\mathbf{U}_D(x; \theta_2) - \mathbf{u}_D(x) \right)^{r_{12}} d\omega_1(x) \right]^{1/r_{12}}.
\end{aligned} \tag{31}$$

According to the inequalities (28) - (31), we conclude

$$\begin{aligned}
& \int_{\Omega_D} \left(|\mathbf{U}_D(x; \theta_2)| \mathbf{U}_D(x; \theta_2) - |\mathbf{u}_D(x)| \mathbf{u}_D(x) \right)^2 d\omega_1(x) \\
& \leq (\epsilon^2 + \sup_{\Omega_D} |\mathbf{u}_D(x)|^2)^2 + \sup_{\Omega_D} |\mathbf{u}_D(x)| \epsilon^2 + 2\epsilon \sup_{\Omega_D} |\mathbf{u}_D(x)| (\epsilon + \sup_{\Omega_D} |\mathbf{u}_D(x)|)^2.
\end{aligned} \tag{32}$$

For the boundary condition, we know

$$\int_{\partial\Omega_D \setminus \Gamma} |\mathbf{U}_D(x; \theta_2) - \mathbf{u}_D(x)|^2 d\omega_2(x) \leq C\epsilon^2. \tag{33}$$

Combining the equations (26) - (33), we obtain

$$\begin{aligned}
J_{\Omega_D \setminus \Gamma}(\bar{\mathbf{U}}) &= \left\| f_D - \nabla \cdot \mathbf{U}_D(x; \theta_2) \right\|_{0, \Omega_D, \omega_1}^2 + \left\| P_D(x; \theta_4) \right\|_{0, \partial\Omega_D \setminus \Gamma, \omega_2}^2 \\
& \quad + \left\| \frac{\mu}{\rho} K^{-1} \mathbf{U}_D(x; \theta_2) + \frac{\beta}{\rho} |\mathbf{U}_D(x; \theta_2)| \mathbf{U}_D(x; \theta_2) + \nabla P_D(x; \theta_4) - \mathbf{g}_D \right\|_{0, \Omega_D, \omega_1}^2 \\
& \leq \int_{\Omega_D} \left| \nabla \cdot \left(\mathbf{U}_D(x; \theta_2) - \mathbf{u}_D(x) \right) \right|^2 d\omega_1(x) + \int_{\partial\Omega_D \setminus \Gamma} \left(P_D(x; \theta_4) - p_D(x) \right)^2 d\omega_2(x) \\
& \quad + \frac{\beta}{\rho} \int_{\Omega_D} \left(|\mathbf{U}_D(x; \theta_2)| \mathbf{U}_D(x; \theta_2) - |\mathbf{u}_D(x)| \mathbf{u}_D(x) \right) d\omega_1(x) \\
& \quad + \frac{\mu}{\rho} K^{-1} \int_{\Omega_D} \left(\mathbf{U}_D(x; \theta_2) - \mathbf{u}_D(x) \right)^2 d\omega_1(x) \\
& \quad + \int_{\Omega_D} \left(\nabla \mathbf{P}_D(x; \theta_4) - \nabla \mathbf{p}_D(x) \right)^2 d\omega_1(x) \\
& \leq C\epsilon^2.
\end{aligned} \tag{34}$$

The loss in interface is referred in (11). According to the Assumption 3.1, we know that

$$\begin{aligned}
& \int_{\Gamma} \left| \nabla \mathbf{U}_D(x; \theta_2) - \nabla \mathbf{u}_D(x) \right|^2 d\omega_3(x) \\
& \leq \int_{\Gamma} \left(|\mathbf{U}_D(x; \theta_2)|^{l_7} + |\mathbf{u}_D(x)|^{l_8} \right) \left(\mathbf{U}_D(x; \theta_2) - \mathbf{u}_D(x) \right)^2 d\omega_3(x),
\end{aligned} \tag{35}$$

which can be updated by using the *Hölder* inequality and *Young* inequality, thus we have

$$\begin{aligned}
& \left[\int_{\Gamma} \left(|\mathbf{U}_D(x; \theta_3)|^{l_7} + |\mathbf{u}_D|^{l_8} \right)^{r_{15}} d\omega_3(x) \right]^{1/r_{15}} \\
& \times \left[\int_{\Gamma} |\mathbf{U}_D(x; \theta_3) - \mathbf{u}_D(x)|^{2r_{16}} d\omega_3(x) \right]^{1/r_{16}} \\
& \leq \left[\int_{\Gamma} \left(|\mathbf{U}_D(x; \theta_3) - \mathbf{u}_D(x)|^{l_7} + |u_D(x)|^{l_7 \vee l_8} \right)^{r_{15}} d\omega_3(x) \right]^{1/r_{15}} \\
& \times \left[\int_{\Gamma} \left(\mathbf{U}_D(x; \theta_3) - \mathbf{u}_D(x) \right)^{2r_{16}} d\omega_3(x) \right]^{1/r_{16}} \\
& \leq C \left(\epsilon^{l_7} + \sup_{\Gamma} |\mathbf{u}_D(x)|^{l_7 \vee l_8} \right) \epsilon^2,
\end{aligned} \tag{36}$$

where $\frac{1}{r_{15}} + \frac{1}{r_{16}} = 1$ and $l_7 \vee l_8 = \max\{l_7, l_8\}$.

Above all, we can obtain

$$\begin{aligned}
J_{\Gamma}(\bar{\mathbf{U}}) &= \left\| \mathbf{U}_S(x; \theta_1) \cdot \mathbf{n}_S - \mathbf{U}_D(x; \theta_2) \cdot \mathbf{n}_S \right\|_{0, \Gamma, \omega_3}^2 + \left\| P_S(x; \theta_3) - \nu \mathbf{n}_S \frac{\partial \mathbf{U}_S(x; \theta_1)}{\partial \mathbf{n}_S} - P_D(x; \theta_4) \right\|_{0, \Gamma, \omega_3}^2 \\
&+ \left\| -\nu \mathbf{t} \frac{\partial \mathbf{U}_S(x; \theta_1)}{\partial \mathbf{n}_S} - G \mathbf{U}_S(x; \theta_1) \cdot \mathbf{t} \right\|_{0, \Gamma, \omega_3}^2 \\
&\leq \left\| \mathbf{U}_S(x; \theta_2) - \mathbf{u}_S(x) \right\|_{0, \Gamma, \omega_3}^2 \left\| \mathbf{n}_S \right\|_{0, \Gamma, \omega_3}^2 + \left\| \mathbf{U}_D(x; \theta_2) - \mathbf{u}_D(x) \right\|_{0, \Gamma, \omega_3}^2 \left\| \mathbf{n}_S \right\|_{0, \Gamma, \omega_3}^2 \\
&+ \left\| P_S(x; \theta_3) - p_S(x) \right\|_{0, \Gamma, \omega_3}^2 + \left\| P_D(x; \theta_4) - p_D(x) \right\|_{0, \Gamma, \omega_3}^2 \\
&+ \nu \left\| \mathbf{n}_S \right\|_{0, \Gamma, \omega_3}^4 \left\| \nabla \mathbf{U}_S(x; \theta_1) - \nabla \mathbf{u}_S(x; \theta_1) \right\|_{0, \Gamma, \omega_3}^2 + G \left\| \mathbf{t} \right\|_{0, \Gamma, \omega_3}^2 \left\| \mathbf{U}_S(x; \theta_1) - \mathbf{u}_S(x) \right\|_{0, \Gamma, \omega_3}^2 \\
&+ \nu \left\| \mathbf{t} \right\|_{0, \Gamma, \omega_3}^2 \left\| \nabla \mathbf{U}_S(x; \theta_1) - \nabla \mathbf{u}_S(x; \theta_1) \right\|_{0, \Gamma, \omega_3}^2 \left\| \mathbf{n}_S \right\|_{0, \Gamma, \omega_3}^2 \\
&\leq C \epsilon^2,
\end{aligned} \tag{37}$$

which completes the proof. \square

3.2 Convergence of the CDNNs to the exact solution

In the last subsection, we have proved the convergence of the loss function. In this subsection, we remain to discuss the convergence of the CDNNs to the exact solution. According to the Galerkin

method, the neural networks satisfy

$$\nabla \cdot \mathbf{U}_D^n - f_D = 0, \quad \text{in } \Omega_D, \quad (38)$$

$$\frac{\mu}{\rho} K^{-1} \mathbf{U}_D^n + \frac{\beta}{\rho} |\mathbf{U}_D^n| \mathbf{U}_D^n + \nabla P_D^n - \mathbf{g}_D = 0, \quad \text{in } \Omega_D, \quad (39)$$

$$P_D^n = 0, \quad \text{on } \partial\Omega_D \setminus \Gamma, \quad (40)$$

$$-\nu \Delta \mathbf{U}_S^n + \nabla P_S^n - \mathbf{f}_S = 0, \quad \text{in } \Omega_S, \quad (41)$$

$$\nabla \cdot \mathbf{U}_S^n = 0, \quad \text{on } \Omega_S, \quad (42)$$

$$\mathbf{U}_S^n = 0, \quad \text{on } \partial\Omega_S \setminus \Gamma, \quad (43)$$

$$\mathbf{U}_S^n \cdot \mathbf{n}_S - \mathbf{U}_D^n \cdot \mathbf{n}_S = 0, \quad \text{on } \Gamma, \quad (44)$$

$$P_S^n - \nu \mathbf{n}_S \frac{\partial \mathbf{U}_S^n}{\partial \mathbf{n}_S} - P_D^n = 0, \quad \text{on } \Gamma, \quad (45)$$

$$-\nu \mathbf{t} \frac{\partial \mathbf{U}_S^n}{\partial \mathbf{n}_S} - G \mathbf{U}_S^n \cdot \mathbf{t} = 0, \quad \text{on } \Gamma. \quad (46)$$

Based on the above system of equations, we give the following assumption and theorem to guarantee the convergency of the CDNNs to the exact solution.

Assumption 3.2. We assume $(\mathbf{u}_S, \mathbf{u}_D) \in C^\xi(\bar{\Omega}_S) \times C^\xi(\bar{\Omega}_D)$ where $\xi > 2$ with itself and its first derivative bounded in $\bar{\Omega}_S \times \bar{\Omega}_D$. Moreover, for every $n \in \mathbb{N}$, $\mathbf{U}_S^n \times \mathbf{U}_D^n \in C^{1,2}(\bar{\Omega}_S) \cap \mathbb{X}_S \times C^{1,2}(\bar{\Omega}_D) \cap L^3(\Omega_D)^2$. We assume that the subspace $\mathbb{X}_S \times L^3(\Omega_D)^2 \times L^2(\Omega_S) \times \mathbb{Y}_D \subset [\mathfrak{C}_{\mathbf{U}_S}(\varphi)]^d \times [\mathfrak{C}_{\mathbf{U}_D}(\zeta)]^d \times \mathfrak{C}_{P_S}(\psi) \times \mathfrak{C}_{P_D}(\gamma)$ satisfies the discrete inf-sup condition.

Theorem 3.2. Under the Assumption 3.1 and Theorem 3.1, the neural network \mathbf{U}_S^n can converge strongly to \mathbf{u}_S in L^2 , P_S^n , \mathbf{U}_D^n and P_D^n can converge strongly to p_S , \mathbf{u}_D and p_D in H^{-1} . In addition, if the sequences $\{\mathbf{U}_S^n\}_{n \in \mathbb{N}}$, $\{P_S^n\}_{n \in \mathbb{N}}$, $\{\mathbf{U}_D^n\}_{n \in \mathbb{N}}$ and $\{P_D^n\}_{n \in \mathbb{N}}$ are uniformly bounded and equicontinuous in Ω_S and Ω_D , they can converge to \mathbf{u}_S , p_S , \mathbf{u}_D and p_D respectively.

Proof. Firstly, we give the weak formulation for (38)-(46). Multiplying (41) by $\mathbf{V}_S^n \in \mathbb{X}_S \cap [\mathfrak{C}_{\mathbf{U}_S}(\varphi)]^d$ and (42) by $Q_S^n \in \mathfrak{C}_{P_S}(\psi)$ and integration by parts yields

$$\nu(\nabla \mathbf{U}_S^n, \nabla \mathbf{V}_S^n)_{\Omega_S} - \nu \langle \nabla \mathbf{U}_S^n \cdot \mathbf{n}_S, \mathbf{V}_S^n \rangle_{\Gamma} - (P_S^n, \nabla \cdot \mathbf{V}_S^n)_{\Omega_S} + \langle P_S^n, \mathbf{V}_S^n \cdot \mathbf{n}_S \rangle_{\Gamma} = (\mathbf{f}_S, \mathbf{V}_S^n)_{\Omega_S}, \quad (47)$$

$$(\nabla \cdot \mathbf{U}_S^n, Q_S^n)_{\Omega_S} = 0. \quad (48)$$

Multiplying (38) by $Q_D^n \in \mathbb{Y}_D \cap \mathfrak{C}_{P_D}(\gamma)$ and (39) by $\mathbf{V}_D^n \in [\mathfrak{C}_{\mathbf{U}_D}(\zeta)]^d$, it then follows from integration by parts that

$$-(\mathbf{U}_D^n, \nabla \mathbf{Q}_D^n)_{\Omega_D} + \langle \mathbf{U}_D^n \cdot \mathbf{n}_D, \mathbf{Q}_D^n \rangle_{\Gamma} = (f_D, \mathbf{Q}_D^n)_{\Omega_D}, \quad (49)$$

$$\frac{\mu}{\rho} (K^{-1} \mathbf{U}_D^n, \mathbf{V}_D^n)_{\Omega_D} + \frac{\beta}{\rho} (|\mathbf{U}_D^n| \mathbf{U}_D^n, \mathbf{V}_D^n)_{\Omega_D} - (P_D^n, \nabla \cdot \mathbf{V}_D^n)_{\Omega_D} + \langle P_D^n, \mathbf{V}_D^n \cdot \mathbf{n}_D \rangle_{\Gamma} = (\mathbf{g}_D, \mathbf{V}_D^n)_{\Omega_D}. \quad (50)$$

Considering the interface conditions, simple algebraic calculation yields

$$\langle \nabla \mathbf{U}_S^n \mathbf{n}_S, \mathbf{V}_S^n \rangle_\Gamma = \langle \mathbf{n}_S \nabla \mathbf{U}_S^n \cdot \mathbf{n}_S, \mathbf{V}_S^n \cdot \mathbf{n}_S \rangle_\Gamma + \langle \mathbf{n}_S \nabla \mathbf{U}_S^n \cdot \mathbf{t}, \mathbf{V}_S^n \cdot \mathbf{t} \rangle_\Gamma$$

which gives by employing interface conditions (45) and (46)

$$\langle (P_S^n I - \nu \nabla \mathbf{U}_S^n) \mathbf{n}_S, \mathbf{V}_S^n \rangle_\Gamma = \langle P_D^n, \mathbf{V}_S^n \cdot \mathbf{n}_S \rangle_\Gamma + G \langle \mathbf{U}_S^n \cdot \mathbf{t}, \mathbf{V}_S^n \cdot \mathbf{t} \rangle_\Gamma. \quad (51)$$

For convenience of presentation, we introduce the nonlinear operator $A : L^3(\Omega_D)^2 \rightarrow L^{3/2}(\Omega_D)^2$ defined by

$$A(\mathbf{V}) = \frac{\mu K^{-1}}{\rho} \mathbf{V} + \frac{\beta}{\rho} |\mathbf{V}| \mathbf{V}. \quad (52)$$

The definition of (52) gives

$$(A(\mathbf{U}_D^n), \mathbf{U}_D^n)_{\Omega_D} \geq C(\|\mathbf{U}_D^n\|_0^2 + \|\mathbf{U}_D^n\|_{L^3}^3).$$

According to the Assumption 3.2 and (50),

$$\begin{aligned} \|P_D^n\|_0 &\leq C \sup_{\mathbf{V}_D^n \in L^3(\Omega_D)^2 \cap [\mathbf{e}_{\mathbf{U}_D}(\zeta)]^d} \frac{(A(\mathbf{U}_D^n), \mathbf{V}_D^n)_{\Omega_D} - (g_D, \mathbf{V}_D^n)_{\Omega_D}}{\|\mathbf{V}_D^n\|_{L^3(\Omega_D)}} \\ &\leq C(\|\mathbf{U}_D^n\|_0 + \|\mathbf{U}_D^n\|_{L^3}^2 + \|g_D\|_0). \end{aligned}$$

Taking $\mathbf{V}_S^n = \mathbf{U}_S^n$, $Q_S^n = P_S^n$, $\mathbf{V}_D^n = \mathbf{U}_D^n$ and $Q_D^n = P_D^n$ in (47)-(50) and adding the resulting equations (51) yields

$$\begin{aligned} &\nu(\nabla \mathbf{U}_S^n, \nabla \mathbf{U}_S^n)_{\Omega_S} + G \langle \mathbf{U}_S^n \cdot \mathbf{t}, \mathbf{U}_S^n \cdot \mathbf{t} \rangle_\Gamma + \frac{1}{2} (A(\mathbf{U}_D^n), \mathbf{U}_D^n)_{\Omega_D} \\ &= (\mathbf{f}_S, \mathbf{U}_S^n)_{\Omega_S} + (f_D, P_D^n)_{\Omega_D} + \frac{1}{2} (g_D, \mathbf{U}_D^n)_{\Omega_D}. \end{aligned}$$

According to the definition of the H^1 norm, the *Young* inequality and the *Poincaré* inequality, we can obtain

$$\begin{aligned} &\|\mathbf{U}_S^n\|_1^2 + \|\mathbf{U}_D^n\|_0^2 + \|\mathbf{U}_D^n\|_{L^3}^3 \\ &\leq C(\|\mathbf{f}_S\|_0 \|\mathbf{U}_S^n\|_0 + \|f_D\|_0 \|P_D^n\|_0 + \|g_D\|_0 \|\mathbf{U}_D^n\|_0) \\ &\leq C(\|\mathbf{f}_S\|_0 \|\mathbf{U}_S^n\|_0 + \|f_D\|_0 (\|\mathbf{U}_D^n\|_0 + \|\mathbf{U}_D^n\|_{L^3}^2 + \|g_D\|_0) + \|g_D\|_0 \|\mathbf{U}_D^n\|_0) \\ &\leq C(\|f_D\|_0^2 + \|f_D\|_0^3 + \|\mathbf{f}_S\|_0^2 + \|g_D\|_0^2). \end{aligned}$$

Thus we have

$$\begin{aligned} \|P_D^n\|_0 &\leq C(\|\mathbf{U}_D^n\|_0 + \|\mathbf{U}_D^n\|_{L^3}^2 + \|g_D\|_0) \\ &\leq C(\|f_D\|_0 + \|f_D\|_0^2 + \|\mathbf{f}_S\|_0 + \|\mathbf{f}_S\|_0^2 + \|g_D\|_0 + \|g_D\|_0^2). \end{aligned}$$

According to the Assumption 3.2, (47) - (48) and (51)

$$\begin{aligned} \|P_S^n\|_0 &\leq C \sup_{\mathbf{V}_S^n \in [\mathbb{X}_S]^2 \cap [\mathbf{c}_{\mathbf{U}_S}(\varphi)]^d} \frac{(\mathbf{f}_S, \mathbf{V}_S^n) - (\nabla \mathbf{U}_S^n, \nabla \mathbf{V}_S^n) - \langle P_D^n, \mathbf{V}_S^n \cdot \mathbf{n}_S \rangle_\Gamma - G \langle \mathbf{U}_S^n \cdot \mathbf{t}, \mathbf{V}_S^n \cdot \mathbf{t} \rangle_\Gamma}{\|\mathbf{V}_S^n\|_0} \\ &\leq C(\|\mathbf{f}_S\|_0 + \|\nabla \mathbf{U}_S^n\|_0 + \|P_D^n\|_0 + \|\mathbf{U}_S^n\|_0) \\ &\leq C(\|f_D\|_0 + \|f_D\|_0^2 + \|\mathbf{f}_S\|_0 + \|\mathbf{f}_S\|_0^2 + \|\mathbf{g}_D\|_0 + \|\mathbf{g}_D\|_0^2). \end{aligned}$$

Up to now, we obtain

$$\{\mathbf{U}_S^n\}_{n \in \mathbb{N}} \text{ is uniformly bounded in } H^1(\Omega_S). \quad (53)$$

By using the uniform boundedness of \mathbf{U}_S^n , we can extract a subsequence $\{\mathbf{U}_S^n\}_{n \in \mathbb{N}}$ of \mathbf{U}_S^n which converge weakly in $H^1(\Omega_S)$. Due to the compact embedding $H^1(\Omega_S) \hookrightarrow L^2(\Omega_S)$, we have

$$\lim_{n \rightarrow \infty} \|\mathbf{U}_S^n - \mathbf{u}_S\|_{0, \Omega_S} = 0.$$

Similarly, we know $L^3(\Omega_D) \subset L^2(\Omega_D)$, which implies that

$$\{\mathbf{U}_D^n\}_{n \in \mathbb{N}} \text{ is uniformly bounded in } L^2(\Omega_D). \quad (54)$$

Due to the compact embedding $L^2(\Omega_D) \hookrightarrow H^{-1}(\Omega_D)$, we have $\lim_{n \rightarrow \infty} \|\mathbf{U}_D^n - \mathbf{u}_D\|_{-1, \Omega_D} = 0$.

The convergence of the P_S^n and P_D^n as follows

$$\lim_{n \rightarrow \infty} \|P_S^n - P_S\|_{-1, \Omega_S} = 0, \quad \lim_{n \rightarrow \infty} \|P_D^n - p_D\|_{-1, \Omega_D} = 0.$$

For all these reasons, $\{\mathbf{U}_S^n\}_{n \in \mathbb{N}}$ converge strongly to \mathbf{u}_S in L^2 , $\{P_S^n\}_{n \in \mathbb{N}}$, $\{\mathbf{U}_D^n\}_{n \in \mathbb{N}}$ and $\{P_D^n\}_{n \in \mathbb{N}}$ converge strongly to p_S , \mathbf{u}_D and p_D in H^{-1} . More generally, by the well known Arzelà-Ascoli theorem we can conclude that $\{\mathbf{U}_S^n\}_{n \in \mathbb{N}}$, $\{P_S^n\}_{n \in \mathbb{N}}$, $\{\mathbf{U}_D^n\}_{n \in \mathbb{N}}$ and $\{P_D^n\}_{n \in \mathbb{N}}$ converge uniformly to \mathbf{u}_S , p_S , \mathbf{u}_D and p_D respectively. \square

4 Numerical Experiments

The section presents several numerical tests to confirm the proposed theoretical results. We start with three examples with known exact solution to test the efficiency of the proposed method, where the permeability for the third example is highly oscillatory. Then, the fourth example with no exact solution shows the application of the proposed method to high contrast permeability problem. This section concludes with a physical flow. The numerical examples presented below could violate the interface conditions (8) and (9) [47], that is, (8) and (9) are replaced by

$$p_S - \nu \mathbf{n}_S \frac{\partial \mathbf{u}_S}{\partial \mathbf{n}_S} = p_D + g_1, \quad \text{on } \Gamma, \quad (55)$$

$$-\nu \mathbf{t} \frac{\partial \mathbf{u}_S}{\partial \mathbf{n}_S} = G \mathbf{u}_S \cdot \mathbf{t} + g_2, \quad \text{on } \Gamma, \quad (56)$$

to deal with this case, the variational formulation has only a small change: The equation 51 now includes the two terms $-\langle g_1, \mathbf{V}_S \cdot \mathbf{n}_S \rangle_\Gamma - \langle g_2, \mathbf{V}_S \cdot \mathbf{t} \rangle_\Gamma$ on the right side. In addition,

Table 1: The relative errors of Test 1.

400 sampled points				
1 layer	\mathbf{U}_S	P_S	\mathbf{U}_D	P_D
$errL^1$	2.49×10^0	9.15×10^0	8.72×10^0	2.74×10^{-1}
$errL^2$	4.84×10^0	9.42×10^0	1.94×10^0	2.99×10^{-1}
2 layers	\mathbf{U}_S	P_S	\mathbf{U}_D	P_D
$errL^1$	4.85×10^{-1}	3.59×10^0	9.62×10^{-2}	4.03×10^{-2}
$errL^2$	9.01×10^{-1}	3.21×10^0	2.19×10^{-1}	4.18×10^{-2}
3 layers	\mathbf{U}_S	P_S	\mathbf{U}_D	P_D
$errL^1$	5.80×10^{-3}	5.26×10^{-2}	1.01×10^{-2}	3.25×10^{-3}
$errL^2$	1.09×10^{-2}	4.66×10^{-2}	2.29×10^{-2}	3.38×10^{-3}

we utilize 16 neurons in each hidden layer and apply the relative L^1 error ($errL^1 : \frac{\|\mathbf{r}-\mathbf{R}\|_{L^1}}{\|\mathbf{r}\|_{L^1}}$) and relative L^2 error ($errL^2 : \frac{\|\mathbf{r}-\mathbf{R}\|_0}{\|\mathbf{r}\|_0}$) to reflect the accuracy between the results of the CDNNs and the exact solution (\mathbf{r} : the exact solution; \mathbf{R} : the neural network).

4.1 Test 1

In this subsection we study the performance of the CDNNs for the benchmark problem presented in [47]. This problem is defined for $\Omega_S = (0, 1)^2$, $\Omega_D = (0, 1) \times (1, 2)$ and the interface $\Gamma = \{0 < x < 1, y = 1\}$ as

$$\mathbf{u}_S = \begin{pmatrix} x^2 \pi \sin(2\pi y)(x-1)^2 \\ -2x \sin(y\pi)^2(2x-1)(x-1) \end{pmatrix}, \quad p_S = (\cos(1) - 1)\sin(1) + \cos(y)\sin(x)$$

and

$$\mathbf{u}_D = \begin{pmatrix} \sin(\pi x)\sin(\pi y) \\ -2x \sin(y\pi)^2(2x-1) \end{pmatrix}, \quad p_D = \sin(\pi x)\cos(\pi y).$$

Similar to [47], we fix \mathbf{K} to be the identity tensor in $\mathbb{R}^{2 \times 2}$, $\mu = \rho = \beta = \nu = 1$. Due to the interface conditions (8) and (9) are violated, we exploit the interface conditions (55) and (56), where g_1 and g_2 can be computed by the exact solution. Specifically, the errors converge as the hidden layer increases in Figure 3(a). Figure 3(b) reveals that the change of data has no significant influence on errors once the size is larger than 10^2 . In particular, Figures 4 - 5 and Table 1 show the details of the results, this is consistent with our theory.

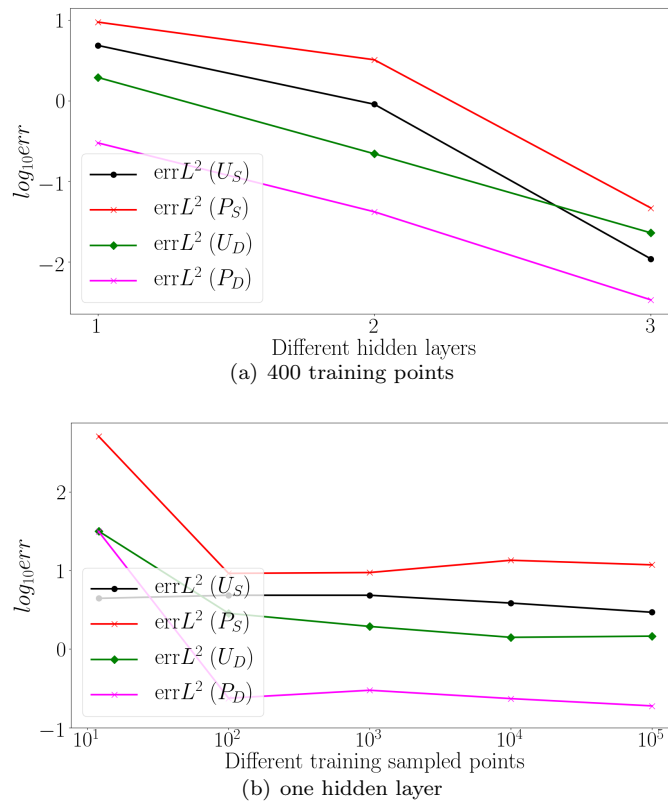


Figure 3: The influence of different hidden layers and different training data on $\text{err}L^2$ (Test 1).

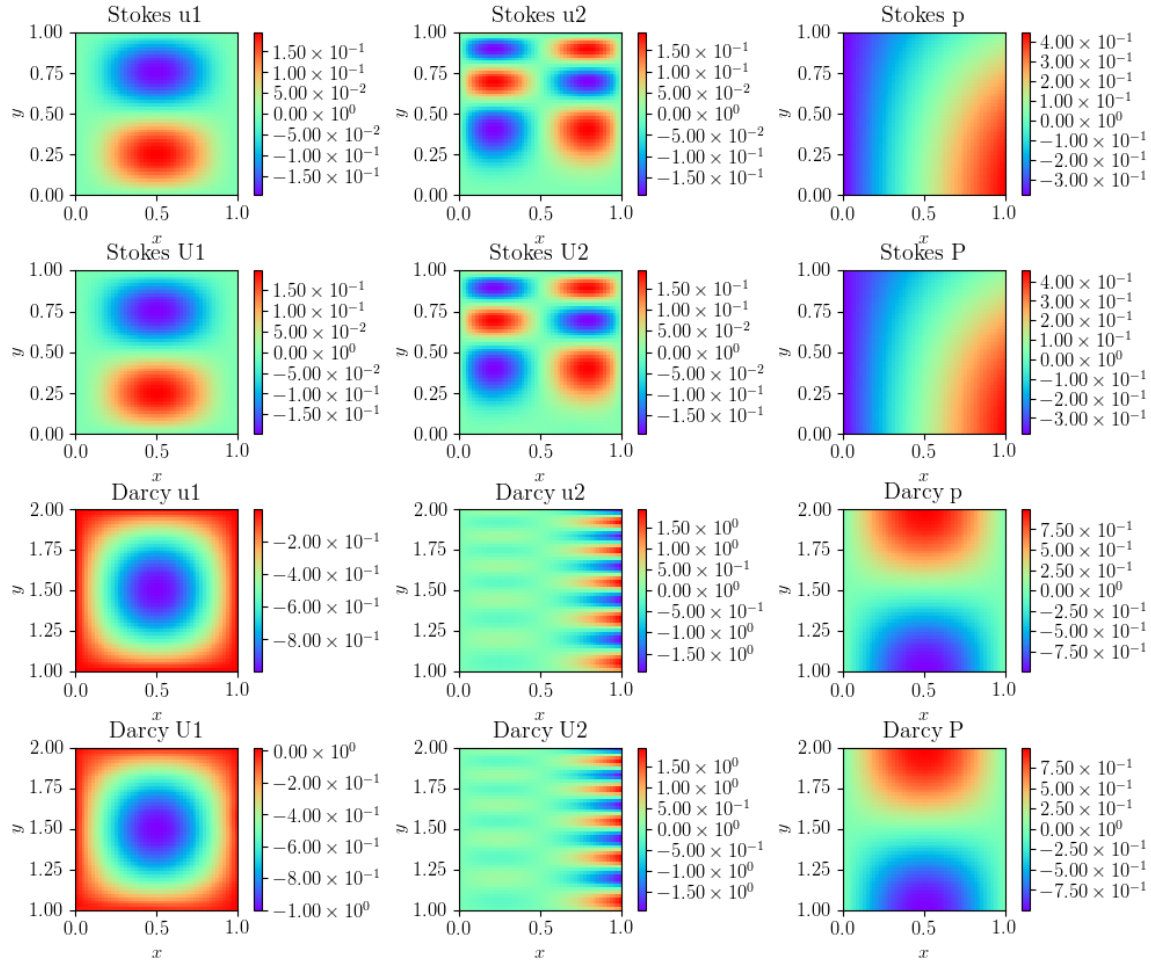


Figure 4: The contrast of the exact solution and the CDNNs (Test 1).

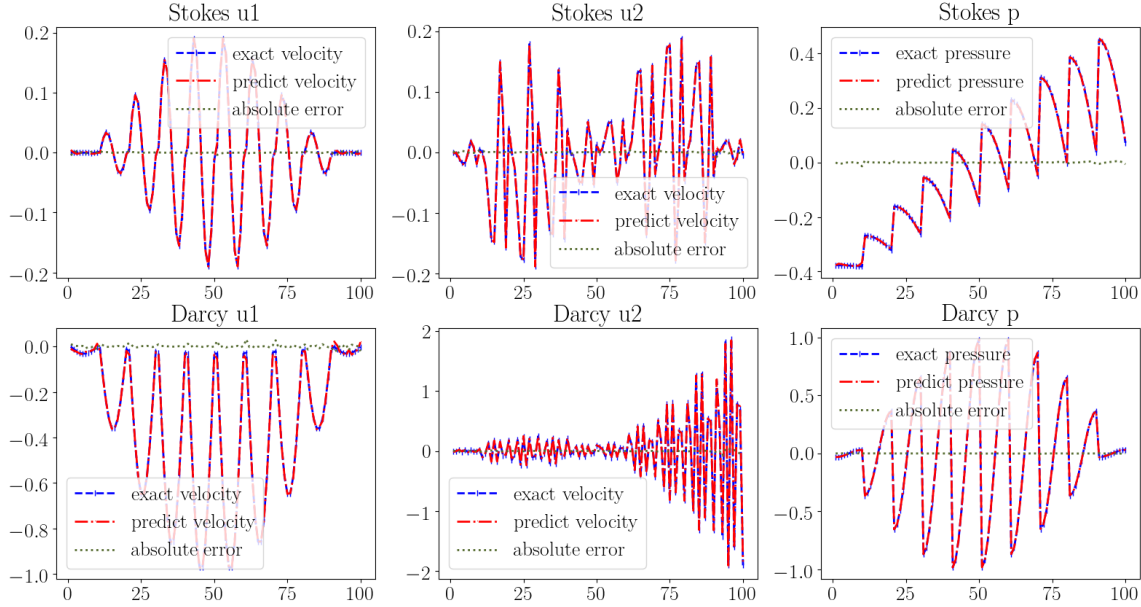


Figure 5: The point-wise errors (Test 1).

4.2 Test 2

In this example, we consider $\Omega_S = (0, 1)^2$, $\Omega_D = (0, 1) \times (1, 2)$ and the interface $\Gamma = \{0 < x < 1, y = 1\}$ with an analytical solution presented in [47]. We set \mathbf{K} to be the identity tensor in $\mathbb{R}^{2 \times 2}$, $\mu = \rho = \beta = \nu = 1$, and the exact solution is given by

$$\mathbf{u}_S = \begin{pmatrix} -\cos^2(\frac{\pi y}{2})\sin(\frac{\pi x}{2}) \\ \frac{1}{4}\cos(\frac{\pi x}{2})(\sin(\pi y) + \pi y) \end{pmatrix}, \quad p_S = \frac{\pi}{4}\cos(\frac{\pi x}{2})(y - 2\cos(\frac{\pi y}{2})^2)$$

and

$$\mathbf{u}_D = \begin{pmatrix} -\frac{1}{8}\sin(\frac{\pi x}{2}) \\ \frac{1}{4}\pi\cos(\frac{\pi x}{2}) \end{pmatrix}, \quad p_D = -\frac{\pi}{4}\cos(\frac{\pi x}{2})y.$$

Naturally, the corresponding \mathbf{f}_S , f_D , and \mathbf{g}_D can be calculated by the exact solution. Note that this example satisfies the interface conditions (7) - (9). According to Test 1, we choose appropriate data and hidden layer to solve the second example. Figures 6 - 7 and Table 2 show the accuracy of the CDNNs for solving the coupled problems in detail.

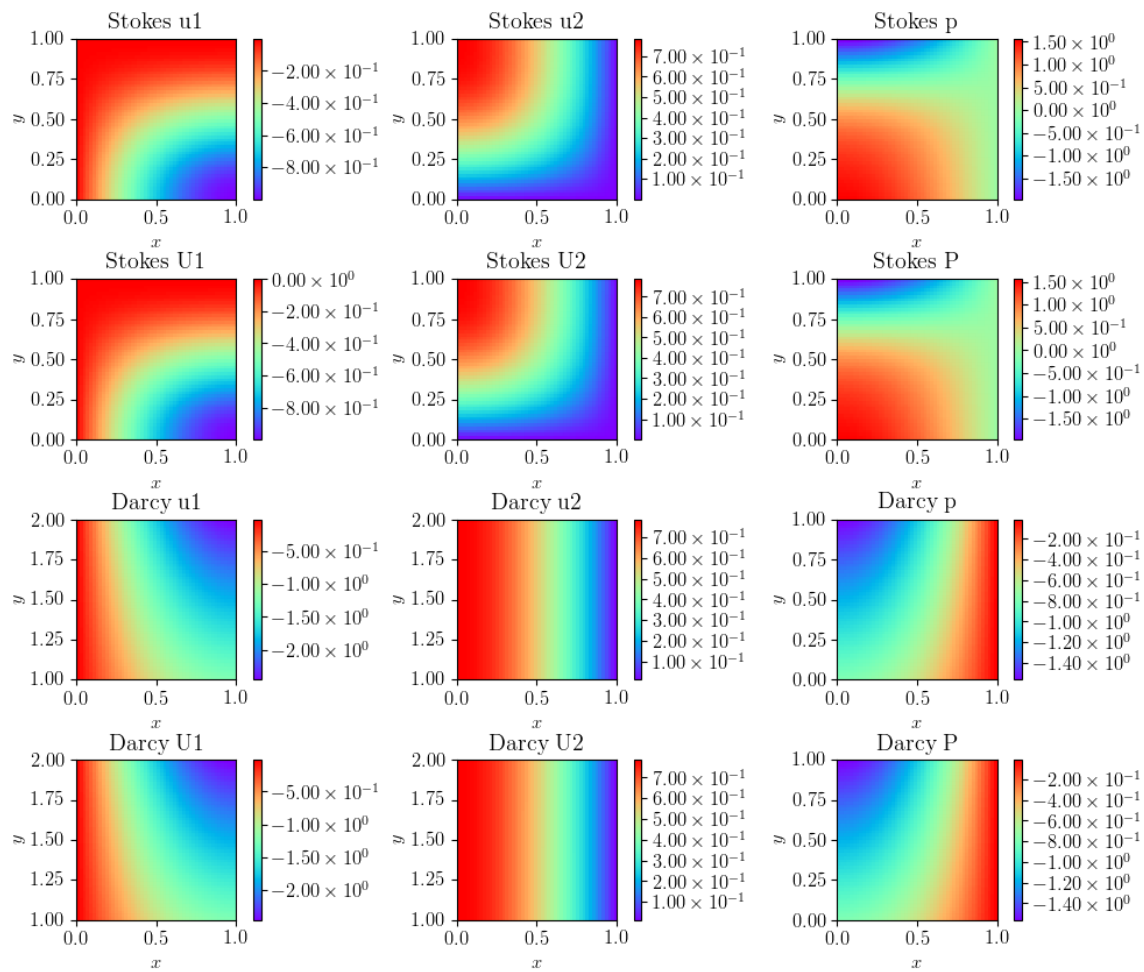


Figure 6: The contrast of the exact solution and the results of the CDNNs (Test 2).

Table 2: The relative errors of Test 2.

400 sampled points				
1 layer	\mathbf{U}_S	P_S	\mathbf{U}_D	P_D
$errL^1$	1.82×10^{-2}	1.19×10^{-1}	1.57×10^{-2}	1.08×10^{-2}
$errL^2$	3.66×10^{-2}	1.23×10^{-1}	4.62×10^{-2}	1.11×10^{-2}
2 layers	\mathbf{U}_S	P_S	\mathbf{U}_D	P_D
$errL^1$	2.27×10^{-4}	1.74×10^{-3}	1.04×10^{-4}	4.67×10^{-5}
$errL^2$	4.21×10^{-4}	2.00×10^{-3}	3.18×10^{-4}	5.55×10^{-5}
3 layers	\mathbf{U}_S	P_S	\mathbf{U}_D	P_D
$errL^1$	1.65×10^{-4}	1.01×10^{-3}	1.13×10^{-4}	7.69×10^{-5}
$errL^2$	3.37×10^{-4}	1.50×10^{-3}	3.44×10^{-4}	8.32×10^{-5}

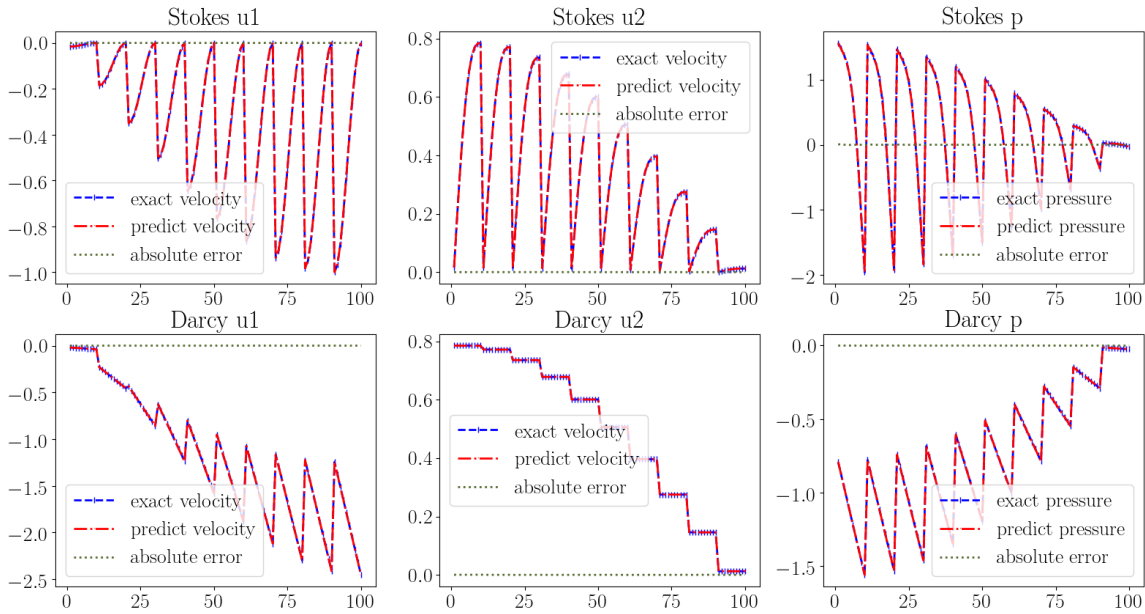


Figure 7: The point-wise errors (Test 2).

4.3 Test 3

In this subsection, we solve coupling of the Stokes and Darcy-Forchheimer problems with highly oscillatory permeability over domains $\Omega_S = (0, 1) \times (0, 1/2)$, $\Omega_D = (0, 1) \times (1/2, 1)$ and the interface $\Gamma = \{0 < x < 1, y = 1/2\}$ presented in [47]. Here we set $\mu = \rho = \beta = \nu = 1$, $K^{-1} = \varrho I$ and ϱ is

defined by

$$\varrho = \frac{2 + 1.8\sin(2\pi x/\varepsilon)}{2 + 1.8\sin(2\pi y/\varepsilon)} + \frac{2 + 1.8\sin(2\pi y/\varepsilon)}{2 + 1.8\sin(2\pi x/\varepsilon)},$$

where $\varepsilon = 1/16$. The profile of ϱ is shown in Figure 8. The exact solution is given by

$$\mathbf{u}_S = \begin{pmatrix} 16y\cos(\pi x)^2(y^2 - 0.25) \\ 8\pi\cos(\pi x)\sin(\pi x)(y^2 - 0.25)^2 \end{pmatrix}, \quad p_S = x^2$$

and

$$\mathbf{u}_D = \begin{pmatrix} \sin(2\pi x)\cos(2\pi y) \\ -\cos(2\pi x)\sin(2\pi y) \end{pmatrix}, \quad p_D = \cos(2\pi x)\cos(2\pi y).$$

We calculate the relative errors in Table 3 to reflect ability of the CDNNs for solving the coupled problems with highly oscillatory permeability. Figures 9 - 10 reveal that the CDNNs handle the highly oscillatory permeability coupled problems without losing accuracy.

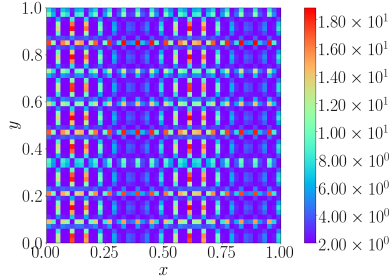


Figure 8: The value of ϱ (Test 3).

Table 3: The relative errors of Test 3.

400 sampled points				
1 layer	\mathbf{U}_S	P_S	\mathbf{U}_D	P_D
$errL^1$	3.59×10^{-1}	5.03×10^0	5.52×10^{-2}	7.59×10^{-2}
$errL^2$	6.79×10^{-1}	5.20×10^0	1.73×10^{-1}	7.07×10^{-2}
2 layers	\mathbf{U}_S	P_S	\mathbf{U}_D	P_D
$errL^1$	8.42×10^{-4}	9.41×10^{-3}	1.15×10^{-3}	1.32×10^{-3}
$errL^2$	1.65×10^{-3}	1.05×10^{-2}	3.43×10^{-3}	1.56×10^{-3}
3 layers	\mathbf{U}_S	P_S	\mathbf{U}_D	P_D
$errL^1$	1.89×10^{-4}	3.04×10^{-3}	2.97×10^{-4}	6.70×10^{-5}
$errL^2$	3.65×10^{-4}	3.37×10^{-3}	8.98×10^{-4}	8.40×10^{-5}

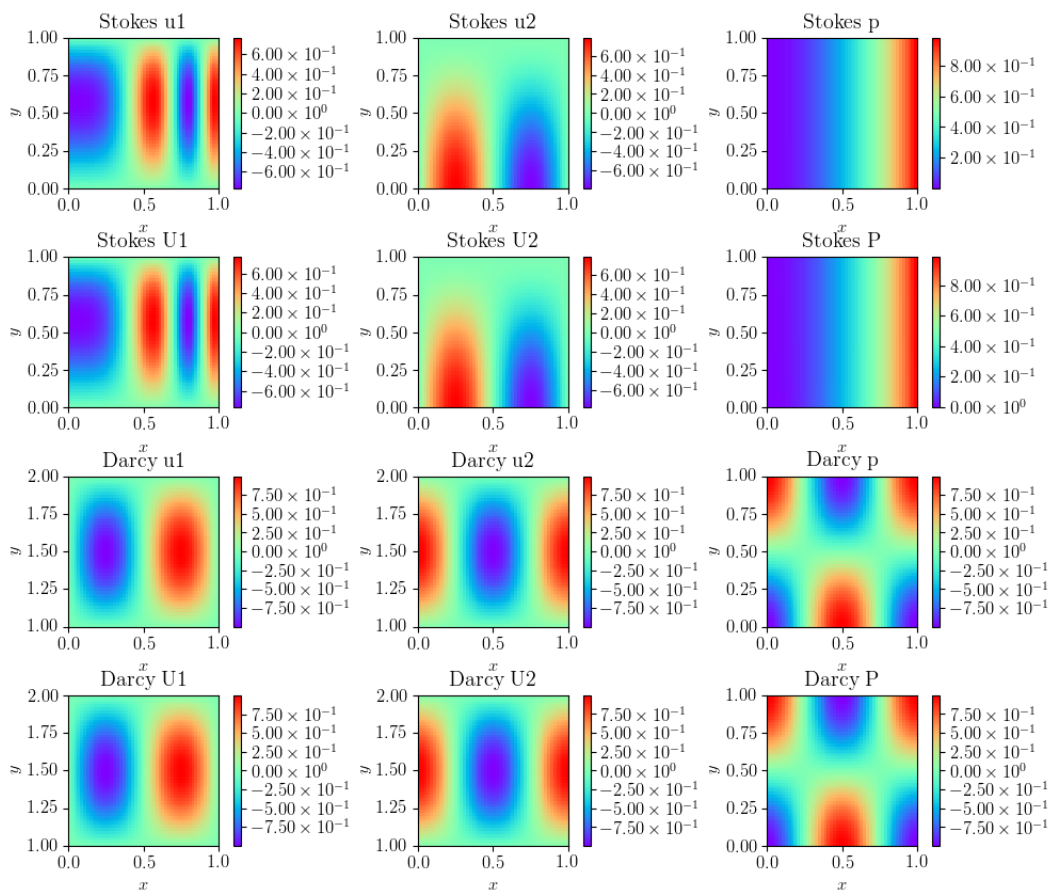


Figure 9: The contrast of the exact solution and the results of the CDNNs (Test 3).

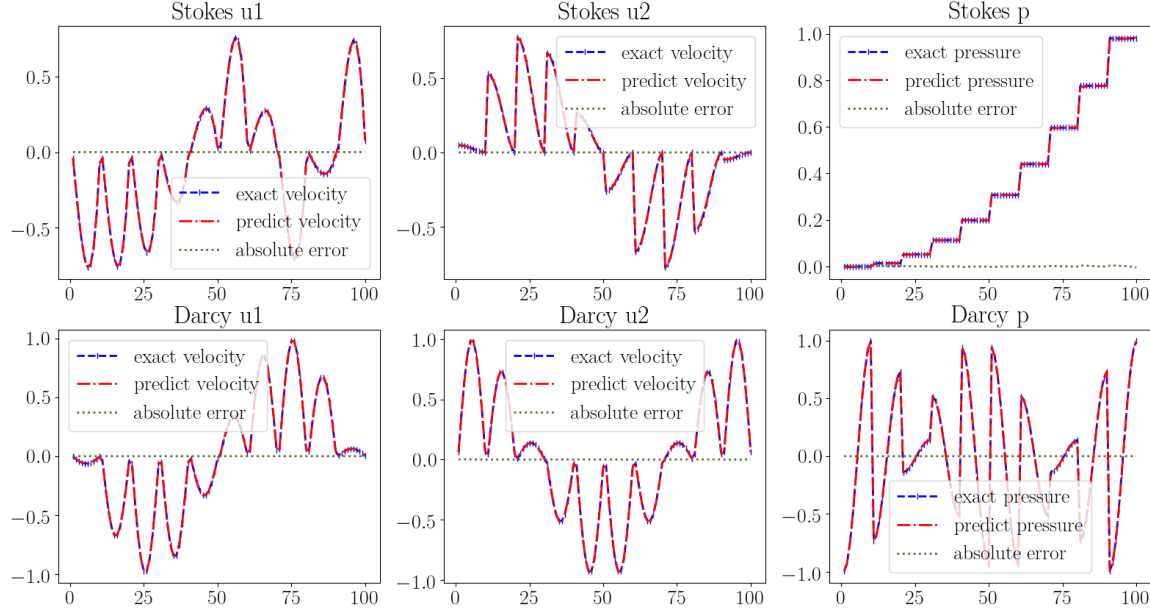


Figure 10: The point-wise errors (Test 3).

4.4 Test 4

The problems that we have studied so far have the exact solution. In this example, we consider coupling of the Stokes and Darcy-Forchheimer problems with no exact solution over $\Omega_S = (-1/2, 3/2) \times (0, 2)$, $\Omega_D = (-1/2, 3/2) \times (-2, 0)$ and the interface $\Gamma = \{-1/2 < x < 3/2, y = 0\}$. Specifically, in the Stokes region, the Dirichlet boundary condition is given by Kovasznay flow [48],

$$\mathbf{u}_S = \begin{pmatrix} 1 - e^{\lambda x} \cos(2\pi y) \\ \frac{\lambda}{2\pi} e^{\lambda x} \sin(2\pi y) \end{pmatrix},$$

where $\lambda = \frac{-8\pi^2}{1 + \sqrt{1 + 64\pi^2}}$. Moreover, we set $\mu = \rho = \beta = \nu = 1$ and $\mathbf{g}_D = \mathbf{0}$, $f_D = 0$, $\mathbf{f}_S = \mathbf{0}$. In addition, p_D satisfies the homogeneous Dirichlet boundary condition along $y = -2$, otherwise it has an homogeneous Neumann boundary condition. The permeability is taken to be $K = \varepsilon I$ and the $\varepsilon = 10^4$. Since the exact solution for this example is not available, we provide L^2 error of interface to demonstrate the accuracy of the CDNNs in Table 4. Obviously, the error decreases gradually with the increasing of the hidden layers. Furthermore, Figures 11 - 12 display the exact solution and the results of CDNNs in detail.

Table 4: The error in interface of Test 4 (K=10000).

	400 sampled points		
	<i>Interface1</i>	<i>Interface2</i>	<i>Interface3</i>
1 layer	6.49×10^{-2}	9.14×10^{-2}	3.03×10^{-2}
2 layers	2.31×10^{-2}	4.74×10^{-2}	2.38×10^{-3}
3 layers	2.12×10^{-2}	1.28×10^{-2}	4.94×10^{-4}

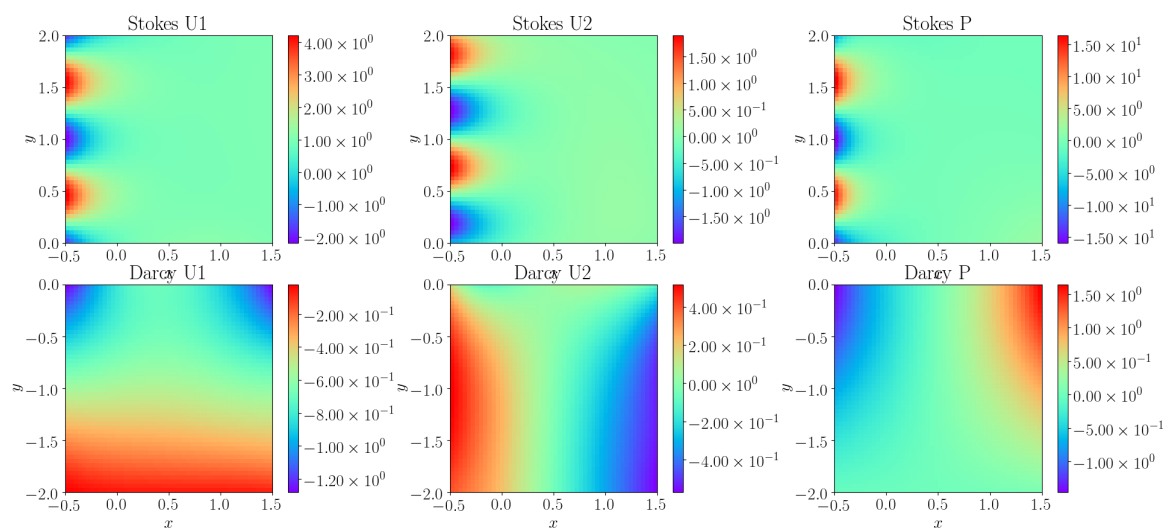


Figure 11: The results of CDNNs (Test 4).

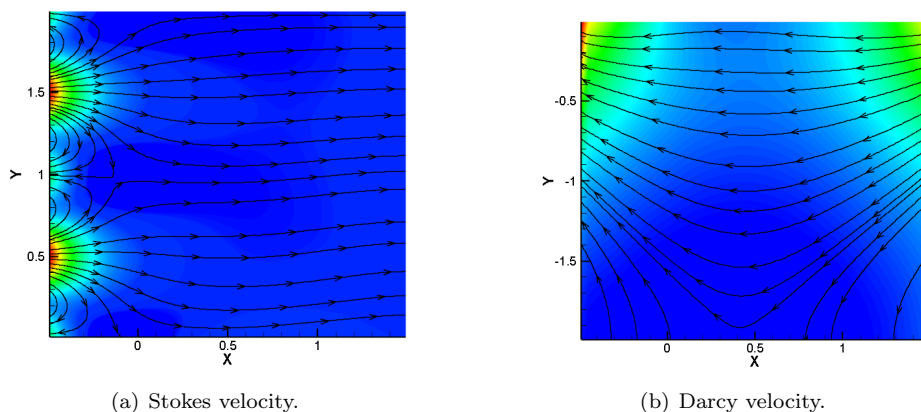


Figure 12: The velocity of Stokes and Darcy (Test 4).

4.5 Test 5

We conclude this section with a physical flow, where $\Omega_S = (0, 1) \times (1, 2)$, $\Omega_D = (0, 1)^2$ and the interface $\Gamma = \{0 < x < 1, y = 1\}$. In Ω_S , the boundaries of the cavity are walls with no-slip condition, except for the upper boundary where a uniform tangential velocity $\mathbf{u}_S(x, 2) = (1, 0)^T$ is imposed, which is driven cavity flow. And more precisely, we enforce homogeneous Neumann and Dirichlet boundary conditions, respectively, on $\Gamma_{D,N} = \{x = 0 \text{ or } y = 0\}$ and $\Gamma_{D,D} = \{x = 1\}$. In addition, we set K to be the identity tensor in $\mathbb{R}^{2 \times 2}$, $\mu = \rho = \beta = \nu = 1$, and $f_D = 0$, $\mathbf{f}_S = \mathbf{0}$, $\mathbf{g}_D = \mathbf{0}$. The results of the CDNNs are depicted in Figure 13. More vividly, we display the velocity flows of free-flow and porous media zones in Figure 13.

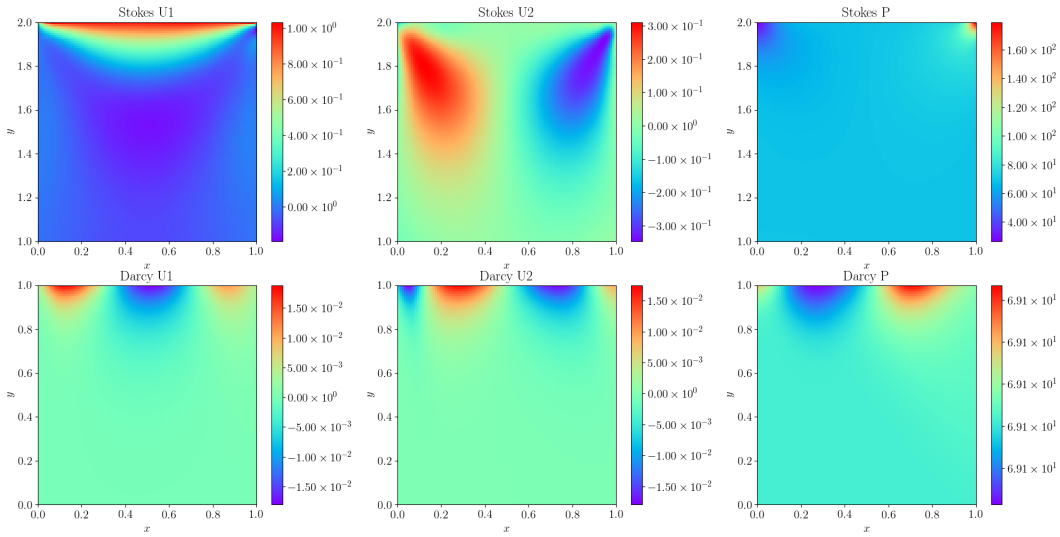
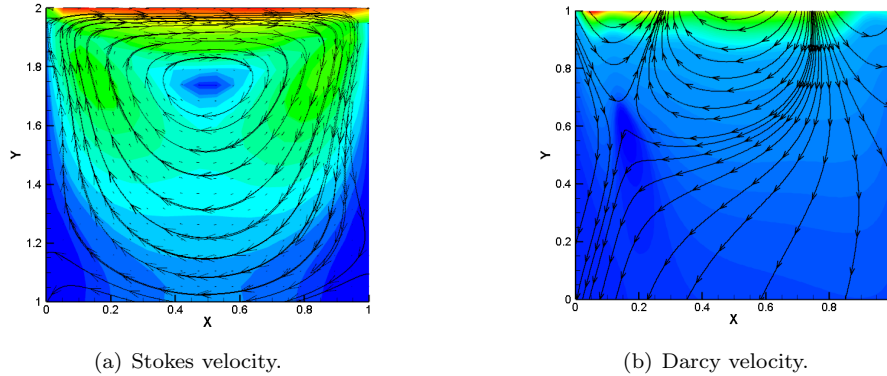


Figure 13: The results of the CDNNs (Test 5).



(a) Stokes velocity.

(b) Darcy velocity.

Figure 14: The velocity flows of Stokes and Darcy (Test 5).

5 Conclusions

In this article, we proposed the CDNNs to study the coupled Stokes and Darcy-Forchheimer problems. This method can avoid many limitations of the traditional methods, such as decoupling, grid construction and the complicated interface conditions. Specially, we provide the convergence of the loss function and the convergence of the CDNNs to the exact solution. The numerical results are consistent with our theory sufficiently. Moreover, we leave the following issues subject to our future works, 1) Combining data-driven with model-driven to solve the high dimensional coupled problems; 2) Considering the specific size of the networks through theoretical analysis; 3) Combining traditional numerical methods with deep learning to solve more complicated high dimensional coupled problems.

References

- [1] P. G. Saffman, On the boundary condition at the surface of a porous medium[J], *Studies in Applied Mathematics*, 1971 (50): 93-101.
- [2] P. Forchheimer, Wasserbewegung durch Boden[J], *Zeitz Vereines Deutsch Ingenieure*, 1901 (45): 1782-1788.
- [3] E. J. Park, Mixed finite element methods for nonlinear second order elliptic problems[J], *SIAM Journal on Numerical Analysis*, 1995 (32): 865-885.
- [4] M. Y. Kim and E. J. park, Fully discrete mixed finite element approximations for non-Darcy flows in porous media[J], *Computers and Mathematics with Applications*, 1999 (38): 113-129.
- [5] E. J. Park, Mixed finite element methods for generalized Forchheimer flow in porous media[J], *Numerical Methods for Partial Differential Equations*, 2005 (21): 213-228.
- [6] M. Discacciati, E. Miglio, and A. Quarteroni, Mathematical and numerical models for coupling surface and groundwater flows[J], *Applied Numerical Mathematics*, 2002 (43): 57-74.
- [7] W. J. Layton, F. Schieweck, and I. Yotov, Coupling fluid flow with porous media flow[J], *SIAM Journal on Numerical Analysis*, 2003 (40): 2195-2218.
- [8] B. Rivière , Analysis of a discontinuous finite element method for the coupled Stokes and Darcy problems[J], *Journal of Scientific Computing*, 2005 (22): 479-500.
- [9] B. Rivière and I. Yotov, Locally conservative coupling of Stokes and Darcy flows[J], *SIAM Journal on Numerical Analysis*, 2005 (42): 1959-1977.
- [10] E. Burman and P. Hansbo, A unified stabilized method for Stokes' and Darcy's equations[J], *Journal of Computational and Applied Mathematics*, 2007 (198): 35-51.

- [11] G. N. Gatica, R. Oyarzúa, and F. J. Sayas, Analysis of fully mixed finite element methods for the Stokes-Darcy coupled problem[J], *Mathematics of Computation*, 2001 (80): 1911-1948.
- [12] V. Girault, D. Vassilev, and I. Yotov, Mortar multiscale finite element methods for Stokes-Darcy flows[J], *Numerische Mathematik*, 2014 (127): 93-165.
- [13] K. Lipnikov, D. Vassilev, and I. Yotov, Discontinuous Galerkin and mimetic finite difference methods for coupled Stokes-Darcy flows on polygonal and polyhedral grids[J], *Numerische Mathematik*, 2014 (126): 321-360.
- [14] A. Krizhevsky, I. Sutskever, G.E. Hinton, Imagenet classification with deep convolutional neural networks[J], *Advances in Neural Information Processing Systems*. 2012: 1097-1105.
- [15] G. Hinton, L. Deng, D. Yu, G.E. Dahl, A. rahman Mohamed, N. Jaitly, A. Senior, Approximation capabilities of multilayer feedforward networks[J], *IEEE Signal Processing Magazine*. 2012 (29): 82-97.
- [16] K. He, X. Zhang, S. Ren, J. Sun, Deep residual learning for image recognition[J], *Proceedings of the IEEE Conference on Computer Vision and Pattern Recognition*, 2016: 770-778.
- [17] N. E. Cotter, The Stone-Weierstrass theorem and its application to neural networks[J]. *IEEE Transaction on Neural Networks*. 1990, 1 (4): 290-295.
- [18] K. Hornik, M. Stinchcombe and H. White, Multilayer feedforward networks are universal approximators[J]. *Neural Networks*. 1989, 2 (5): 359-366.
- [19] K. Hornik, M. Stinchcombe and H. White, Universal approximation of an unknown mapping and its derivatives using multilayer feedforward networks[J]. *Neural Networks*. 1990: 3(5): 551-560.
- [20] K. Hornik, Approximation capabilities of multilayer feedforward networks[J], *Neural Networks*. 1991 (4): 251-257.
- [21] G. Cybenko, Approximations by superpositions of sigmoidal functions[J], *Mathematics of Control, Signals, and Systems*. 1989 (2): 303-314.
- [22] B. C. Csáji, *Approximation With Artificial Neural Networks*[M], Faculty of Sciences, Eötvös Loránd University, 2001.
- [23] M. Telgarsky, Benefits of depth in neural networks[J], *Journal of Machine Learning Research: Workshop and Conference Proceedings*. 2016 (49): 1-23.
- [24] H. M. Q. Liao, T. Poggio, Learning functions: when is deep better than shallow[J], *arXiv preprint arXiv:1603.00988v4*, 2016. [Online]. Available: <https://arxiv.org/abs/1603.00988>.

- [25] Y. Khoo, J. Lu, L. Ying, Solving parametric PDE problems with artificial neural networks[J], arXiv preprint arXiv:1707.03351, 2017. [Online]. Available: <https://arxiv.org/abs/1707.03351>.
- [26] J. Li, J. Yue, W. Zhang, W. Duan, The Deep Learning Galerkin Method for the General Stokes Equations[J]. arXiv preprint arXiv:2009.11701, 2020. [Online]. Available: <https://arxiv.org/abs/2009.11701>.
- [27] J. Li, W. Zhang and J. Yue, A Deep Learnign Galerkin Method for the Second-order linear elliptic equations[J]. International Journal of Numerical Analysis and Modeling. 2021, 18(4): 427-441.
- [28] J. Yue, J. Li, The Deep Learning Galerkin Method for the unsteady Stokes Equations[J]. Journal of Computational Physics. Under review.
- [29] Y. Fan, L. Lin, L. Ying, L. Zepeda-Núñez, A multiscale neural network based on hierarchical matrices[J], arXiv preprint arXiv:1807.01883, 2018. [Online]. Available: <https://arxiv.org/abs/1807.01883>.
- [30] M. Wang , S. W. Cheung, E. T. Chung, et al. , Prediction of discretization of gms-fem using deep learning[J], arXiv preprint arXiv: 1810.12245, 2018. [Online]. Available: <https://arxiv.org/abs/1810.12245>.
- [31] X. Li, Simultaneous approximations of multivariate functions and their derivatives by neural networks with one hidden layer[J]. Neurocomputing. 1996, 12(4): 327-343.
- [32] I. E. Lagaris, A. C. Likas and D. I. Fotiadis, Artificial neural networks for solving ordinary and partial differential equations[J]. IEEE Transaction on Neural Networks. 1998, 9(5): 987-1000.
- [33] I. E. Lagaris, A. C. Likas and D. G. Papageorgiou, Neural-network methods for boundary value problems with irregular boundaries[J]. IEEE Transaction on Neural Networks. 2000, 11(5): 1041-1049.
- [34] K. S. McFall and J. R. Mahan, Artificial neural network method for solution of boundary value problems with exact satisfaction of arbitrary boundary conditions[J]. IEEE Transaction on Neural Networks. 2009, 20(8): 1221-1233.
- [35] M. Raissi, P. Perdikaris and G. E. Karniadakis, Physics informed deep learning (Part I): Data-driven solutions of nonlinear partial differential equations[J]. 2017, arXiv:1711.10561. [Online]. Available: <https://arxiv.org/abs/1711.10561>.
- [36] M. Raissi, P. Perdikaris and G. E. Karniadakis, Physics informed deep learning (Part II): Data-driven discovery of nonlinear partial differential equations[J]. 2017, arXiv:1711.10566. [Online]. Available: <https://arxiv.org/abs/1711.10566>.

- [37] M. Raissi, P. Perdikaris and G. E. Karniadakis, Physics-informed neural networks: A deep learning framework for solving forward and inverse problems involving nonlinear partial differential equations[J]. *Journal of Computational Physics*. 2019 (378): 686-707.
- [38] L. Yang, X. Meng, G. E. Karniadakis, B-PINNs: Bayesian Physics-Informed Neural Networks for Forward and Inverse PDE Problems with Noisy Data[J]. *Journal of Computational Physics*. 2021 (425): 109913.
- [39] C. Rao, H. Sun and Y. Liu, Physics informed deep learning for computational elastodynamics without labeled data[J]. arXiv: 2006.08472v1. 2020. [Online]. Available: <https://arxiv.org/abs/2006.08472>.
- [40] P. Olivier and R. Fablet. PDE-NetGen 1.0: from symbolic PDE representations of physical processes to trainable neural network representations[J]. arXiv:2002.01029. [Online]. Available: <https://arxiv.org/abs/2002.01029> 2020.
- [41] L. Lu, X. Meng, Z. Mao and G. E. Karniadakis, DEEPXDE: A Deep Learning Library for solving differential equations[J]. *SIAM Review*. 63(1), 208-228.
- [42] Z. Fang and J. Zhan, A Physics-Informed Neural Network Framework for PDEs on 3D Surfaces: Time Independent Problems[J]. *IEEE Access*. 2020 (8): 26328-26335.
- [43] G. Pang, L. Lu and G. E. Karniadakis, fPINNs: Fractional Physics-Informed Neural Networks[J]. *SIAM Journal on Scientific Computing*. 2018, 41(4): A2603-A2626.
- [44] Y. Zhu, N. Zabaras, P.-S. Koutsourelakis, P. Perdikaris, Physics-constrained deep learning for high-dimensional surrogate modeling and uncertainty quantification without labeled data[J], *Journal of Computational Physics*. 2019 (394): 56-81.
- [45] J. Sirignano and K. Spiliopoulos, DGM: A deep learning algorithm for solving partial differential equations[J]. *Journal of Computational Physics*. 2018 (375): 1339-1364.
- [46] G. S. Beaver and D. D. Joseph, Boundary conditions at a naturally imperable wall[J], *Journal of Fluid Mechanics*, 1967 (30): 197-207.
- [47] Zhao L., Chung E., Park E. J., et al. Staggered DG method for coupling of the Stokes and Darcy-Forchheimer problems[J]. *SIAM Journal on Numerical Analysis*. 2019, 59(1): 1-31.
- [48] L. I. G. Kovaszny, Laminar flow behind a two-dimension grid[J], *Mathematical Proceedings of the Cambridge Philosophical Society*, 1948 (44): 58-62.
- [49] Léon Bottou: Stochastic Gradient Tricks, *Neural Networks, Tricks of the Trade, Reloaded*, 430-445, Edited by Grégoire Montavon, Genevieve B. Orr and Klaus-Robert Müller, *Lecture Notes in Computer Science (LNCS 7700)*, Springer, 2012.